

Non-parametric Bayesian Vector Autoregression using Multi-subject Data

Suprateek Kundu*

Department of Biostatistics, The University of Texas MD Anderson Cancer Center
and

Joshua Lukemire

Department of Biostatistics and Bioinformatics, Emory University

November 18, 2021

Abstract

There has been a rich development of vector autoregressive (VAR) models for modeling temporally correlated multivariate outcomes. However, the existing VAR literature has largely focused on single subject parametric analysis, with some recent extensions to multi-subject modeling with known subgroups. Motivated by the need for flexible Bayesian methods that can pool information across heterogeneous samples in an unsupervised manner, we develop a novel class of non-parametric Bayesian VAR models based on heterogeneous multi-subject data. In particular, we propose a product of Dirichlet process mixture priors that enables separate clustering at multiple scales, which result in partially overlapping clusters that provide greater flexibility. We develop several variants of the method to cater to varying levels of heterogeneity. We implement an efficient posterior computation scheme and illustrate posterior consistency properties under reasonable assumptions on the true density. Extensive numerical studies show distinct advantages over competing methods in terms of estimating model parameters and identifying the true clustering and sparsity structures. Our analysis of resting state fMRI data from the Human Connectome Project reveals

*The authors gratefully acknowledge support from NIH awards R01AG071174 and R01MH120299

biologically interpretable differences between distinct fluid intelligence groups, and reproducible parameter estimates. In contrast, single-subject VAR analyses followed by permutation testing result in negligible differences, which is biologically implausible.

Keywords: Dirichlet Process mixtures; spatio-temporal data; functional magnetic resonance imaging; Human Connectome Project; posterior consistency.

1 Introduction

Multivariate time-series data routinely arise in diverse application areas such as finance (Cramer and Miller, 1978), econometrics (Engle and Watson, 1981), spatial-temporal studies (Bradley et al., 2015), and medical imaging (Kundu and Risk, 2021). In order to model such data, a rich body of work on modeling autocorrelations and temporal cross-correlations between variables with multivariate outcomes has been developed, of which vector autoregressive (VAR) models are widely used (Lütkepohl, 2005). Our focus in this paper is on Bayesian VAR modeling, which was initially heavily motivated by econometric research (Doan et al., 1984), and has since seen a rich development (Korobilis, 2013; Gefang, 2014). More recently, Bayesian VAR models have been adopted with increasing prominence in biomedical research including patient-level predictive modeling (Lu et al., 2018) and neuroimaging problems (Gorrostieta et al., 2013; Chiang et al., 2017). However, existing Bayesian VAR literature has primarily focused on methodological and computational developments, with limited theoretical investigations. Recently, Ghosh et al. (2018) addressed this gap by establishing posterior consistency for the autocovariance matrix in parametric Bayesian VAR models based on single subject data.

The vast majority of the Bayesian VAR literature involves Gaussian assumptions and parametric prior specifications that may not be sufficiently flexible in characterizing the underlying probability distributions with non-regular features. For example, it is known that the nature of shocks in econometric analysis may not always be Gaussian (Weise, 1999). Similarly, there is a need for flexible VAR modeling for analyzing heterogenous multi-

subject data in our motivating Human Connectome Project (HCP) neuroimaging study, where parametric VAR models prove inadequate (see Section 5). To bypass parametric constraints, some recent articles relaxed Gaussianity assumptions (Lanne and Lütkepohl, 2010; Jeliazkov, 2013) or proposed non-linear extensions (Dahl and González-Rivera, 2003). Recently, Bayesian nonparametric VAR models were proposed by Kalli and Griffin (2018) involving single subject data, where the mixing weights of the transition density depend on the previous lags. On the other hand, Billio et al. (2019) proposed Dirichlet process mixture of normal-Gamma priors on the VAR autocovariance elements. However, the above approaches were applied to small or moderate dimensional data with limited emphasis on modeling heterogeneity across samples and with negligible or no theoretical investigations.

Existing literature has largely ignored the problem of developing provably flexible nonparametric Bayesian VAR methodology to model heterogeneous multi-subject and matrix-variate data, to our knowledge. Such approaches are desirable over single-subject VAR analyses in terms of being able to pool information across samples in a flexible manner that can accommodate arbitrary probability distributions. It also facilitates robust and reproducible parameter estimates and provides a natural foundation to conduct inferences to test for differences across samples via credible intervals, which may not be straightforward under single-subject analysis. Although there is some literature on parametric VAR modeling of multi-subject data, these existing approaches typically require *apriori* knowledge of class labels (Gorrostieta et al., 2013; Chiang et al., 2017; Kook et al., 2021). Hence, they have a limited ability to accommodate heterogeneity within each class and may result in poor performance when the class labels are mis-specified due to no clear distinction between groups. In designing non-parametric Bayesian VAR models based on heterogeneous multi-subject data, our goal is to provide a more flexible characterisation of heterogeneity via unsupervised clustering that results in theoretical guarantees for inference on the distri-

butions of matrix-variate data under reasonable assumptions. It is also desirable that the proposed methods bypasses any restrictive assumptions such as the presence of replicated samples that share fully identical sets of model parameters, which is routinely assumed in Bayesian non-parametric literature (Tokdar, 2006; Durante et al., 2017). However, such assumptions may not be realistic in high-dimensional applications where samples are often effectively clustered only along a subset of directions with the remaining axes being uninformative for clustering (Agrawal et al., 2005), or where there is reason to suspect differential clustering at different scales as in our motivating neuroimaging applications.

Motivated by the above discussions, we propose a class of novel Bayesian non-parametric VAR models that specify Dirichlet process (DP) mixture priors independently on the different VAR model parameters. Our specification results in a product of Dirichlet process mixture priors that is related to the product of experts model (Hinton, 2002) in the machine learning literature. A key feature of the proposed approach is the ability to allow differential clustering at multiple scales, which enables partially overlapping clusters across samples that share only a subset of common model parameters. The multiscale clustering mechanism bypasses the need to assume replicated samples and hence results in greater flexibility. The use of appropriate base measures in the DP allows shrinkage for the autocovariance elements that facilitates feature selection, and it also enables a low rank representation for the residual covariance that ensures model parsimony. We develop several variants of the approach that differ in terms of prior specifications on the autocovariance matrices and which encourage differential degrees of heterogeneity via different modes of multiscale clustering. Starting from a VAR model that allows limited clustering and greater model parsimony, we eventually develop a variant that is able to independently cluster row-specific parameters, which provides greater flexibility in practical applications.

We develop an efficient and scalable Markov chain Monte Carlo (MCMC) implementa-

tion for the proposed class of models. In addition, we establish posterior consistency results for density estimation under non-parametric Bayesian VAR modeling for multi-subject and matrix-variate data as the number of samples (n) grow to ∞ . Our theoretical results assume a fixed number of time scans T (finite time set-up), which is motivated by practical functional magnetic resonance imaging (fMRI) applications where T routinely lies within a few hundreds at the most. Our finite time set-up is in contrast to theoretical settings in parametric VAR analysis that rely on growing T (Ghosh et al., 2018), which may be better suited for time-series data with higher temporal resolution. The proposed non-parametric Bayesian modeling results in greater flexibility by establishing theoretical guarantees for a wider class of true models and bypasses issues related to model mis-specification that may arise in parametric settings. We note that such theoretical results for VAR models involving matrix-variate data represent non-trivial extensions of the rich theoretical properties established in the Bayesian non-parametric literature for multivariate and scalar i.i.d. outcomes (Tokdar, 2006; Canale and De Blasi, 2017), and is of independent interest. We resolve the significant challenges arising from such theoretical analysis by establishing Kullback-Leibler properties for VAR models, and constructing carefully designed sieves that are shown to satisfy certain entropy bounds and tail prior probability conditions under the product of Dirichlet process mixtures. Moreover, we establish that the theoretical results hold for commonly used base measures that enable straightforward posterior computation.

We illustrate the sharp advantages under the proposed non-parametric Bayesian VAR approach in terms of accurately recovering the true model parameters, inferring the sparsity structure for the autocovariance matrix, and identifying the true clustering patterns, compared to competing state-of-the-art methods. Our analysis of resting state fMRI data from a subset of individuals in the HCP study infers several effective connectivity differences between the high and low fluid intelligence groups that are supported by existing evidence

in literature. Moreover, the analysis under the proposed approach produces biologically reproducible estimates that are consistent across repeated neuroimaging scans from the same samples. In contrast, a single subject VAR analysis is able to identify only one effective connectivity difference across groups, which seems biologically implausible, and has weakly reproducible results across repeated scans. The rest of the article is structured as follows. Section 2 develops the methodology and posterior consistency properties, Section 3 describes the posterior computation, Section 4 reports results from extensive simulation studies, and Section 5 describes our analysis of the HCP data. Section 6 contains additional discussions. Supplementary Materials are provided that contain other relevant details.

2 Methodology

2.1 Proposed Model

Consider the data matrix $X_i = (\mathbf{x}_{i1}, \dots, \mathbf{x}_{iT})$, where \mathbf{x}_{it} represents the $(D \times 1)$ temporally dependent multivariate measurement for the i -th subject at the t -th time point ($i = 1, \dots, n, t = 1, \dots, T$). Note that our model can easily accommodate subject-specific scan lengths (T_i); however we will assume $T_i = T$ from hereon in, to ease the exposition. Throughout, we will also assume a fixed dimension (D), and a pre-specified number of time scans (T), as is typically the case with fMRI experiments. Consider the VAR model:

$$\mathbf{x}_{it} = \sum_{k=1}^{\min\{t-1, K\}} A_{ik} \mathbf{x}_{i,t-1} + \boldsymbol{\epsilon}_{it}, \quad \boldsymbol{\epsilon}_{it} \sim N(\mathbf{0}, \Sigma_i), \quad i = 1, \dots, n, \quad t = 1, \dots, T, \quad (1)$$

where A_{ik} denotes the $D \times D$ matrix of autocovariance parameters for subject i at lag k ($k = 1, \dots, K$), $\Sigma_i \in S_{D \times D}$ denotes the time-invariant residual covariance for subject i , $S_{D \times D}$ denotes the space of all $D \times D$ symmetric positive definite matrices, and the lag order (K) is pre-specified as is standard in the VAR model literature (Ghosh et al., 2018). Model (1) implies that the mean of \mathbf{x}_t depends on $\mathbf{x}_{t-1}, \dots, \mathbf{x}_1$ when $t \leq K$ and on $\mathbf{x}_{t-1}, \dots, \mathbf{x}_{t-K}$

for $t > K$, with $\mathbf{x}_{i1} \sim N(0, \Sigma_i)$ as per convention. As is common in practice, the intercept term is fixed to be zero and not included in (1), which is reasonable for our motivating neuroimaging applications involving centered and pre-processed fMRI data.

In order to understand the properties of (1), it is imperative to note that the likelihood for the i -th sample can be written as a product of conditional densities as

$$L(X_i | \Theta_i, \Sigma_i) = \prod_{t=2}^T \phi_{\Sigma_i} \left(\mathbf{x}_{it} - \sum_{k=1}^{\min\{t-1, K\}} A_{ik} \mathbf{x}_{i,t-k} \right) \times \phi_{\Sigma_i}(\mathbf{x}_{i1}), \quad i = 1, \dots, n, \quad (2)$$

where Θ_i denotes the collection of autocovariance matrices for sample i across lags and $\phi_{\Sigma}(\cdot - \boldsymbol{\mu})$ denotes the density of a D -dimensional normal distribution with mean $\boldsymbol{\mu}$ and covariance Σ . For example, the likelihood for the i th sample under a VAR(2) model may be written as $\prod_{t=3}^T \phi_{\Sigma_i}(\mathbf{x}_{it} - \sum_{k=1}^2 A_{ik} \mathbf{x}_{i,t-k}) \times \phi_{\Sigma_i}(\mathbf{x}_{i2} - A_{i1} \mathbf{x}_{i,1}) \times \phi_{\Sigma_i}(\mathbf{x}_{i1})$. The above likelihood in (2) will be used throughout in our treatment of VAR models. We note that (2) is a different way of representing the likelihood compared to the linear regression framework that is often used in single subject VAR models (Han et al., 2015; Ghosh et al., 2018).

Our goal is to propose suitable priors on the model parameters (Θ_i, Σ_i) in (1) to leverage common patterns of information across samples in an unsupervised and flexible manner. A natural framework for pooling information across subjects is via clustering, which also inherently results in model parsimony that is particularly important in our settings where the number of parameters $\{\Theta_i, \Sigma_i\}$ grow with n . Moreover when borrowing information, it is desirable to avoid the assumption of replicated samples that constrains clusters of subjects to share fully identical sets of parameters and hence fails to respect the heterogeneity within clusters. Additional reduction in the number of distinct model parameters via low rank structures is also desirable, particularly for larger dimensions. Finally, it is appealing to design an approach that enables straightforward posterior computation and results in theoretical guarantees. To this end, we propose a product of DP priors on the

model parameters that arises from independent DP mixture priors imposed separately on the autocovariance parameters and the residual covariance and which results in multiscale clustering. Depending on the manner of the DP prior specification on the autocovariance elements, one can obtain different variants of the proposed method that allow for varying degrees of model parsimony via different patterns of multiscale clustering. We first introduce the product of DP priors below, followed by generalizations to additional variants.

In the following model specifications and ensuing theoretical development, we will omit subscript i as appropriate for notational convenience. We propose the following prior

$$\Theta = \{vec(A_1), \dots, vec(A_K)\} \sim P_\Theta, \quad P_\Theta \sim DP(\alpha_1 P_1^*), \quad \Sigma \sim P_S, \quad P_S \sim DP(\alpha_2 P_2^*), \quad (3)$$

where α_1, α_2 , represent precision parameters in the Dirichlet process, the base measure P_1^* belongs to the space of probability measures \mathcal{P}_1 on $\mathcal{D}_1 = \underbrace{\mathfrak{R}^{D^2 \times 1} \times \dots \times \mathfrak{R}^{D^2 \times 1}}_K$, and the base measure P_2^* belongs to the space of probability measures \mathcal{P}_2 on $\mathcal{D}_2 = S_{D \times D}$. Model (3) specifies unknown distributions P_Θ and P_S on model parameters, that are modeled under DP priors. The resulting product of DP priors in (3) is defined on the space of densities \mathcal{P} with domain $\mathcal{D}_1 \times \mathcal{D}_2$ and may be expressed as $\Pi^*(\Theta, \Sigma) = P_S(\Sigma) \times P_\Theta(\Theta)$. This prior specification translates to a *product of DP mixture of VAR (PDPM-VAR)* models that induces a prior Π on the space of probability densities \mathcal{F} for the data matrix X as follows:

$$\begin{aligned} f_P(X) &= \int \int \prod_{t=1}^T \phi_\Sigma \left(\mathbf{x}_t - \sum_{k=1}^{\min\{t-1, K\}} A_k \mathbf{x}_{t-k} \right) dP_\Theta(\Theta) dP_S(\Sigma) \\ &= \sum_{h_1=1}^{\infty} \sum_{h_\sigma=1}^{\infty} \pi_{h_1} \pi_{\sigma, h_\sigma} \prod_{t=1}^T \phi_{\Sigma_{h_\sigma}} \left(\mathbf{x}_t - \sum_{k=1}^{\min\{t-1, K\}} A_{k, h_1} \mathbf{x}_{t-k} \right), \end{aligned} \quad (4)$$

where the second equality is obtained by Sethuraman's (1994) stick breaking representation with $\pi_{h_1} = \nu_{h_1} \prod_{l_1 < h_1} (1 - \nu_{l_1})$, $\nu_{h_1} \sim Be(1, \alpha_1)$, $\pi_{\sigma, h_\sigma} = \nu_{\sigma, h_\sigma} \prod_{l_2 < h_\sigma} (1 - \nu_{\sigma, l_2})$, $\nu_{\sigma, h_\sigma} \sim Be(1, \alpha_2)$, and further $\Sigma_{h_\sigma} \sim P_2^*$, $(vec(A_{1, h_1}), \dots, vec(A_{K, h_1})) \sim P_1^*$. We consider a broad

class of base measures to study theoretical properties (Section 2.2), but for implementation we focus on specific choices for (P_1^*, P_2^*) that facilitate posterior computations (Section 3).

The proposed product of DP priors models the heterogeneity between samples via multiscale clustering, i.e. separately clustering the autocovariance and the residual covariance matrices. In addition to fully distinct clusters with no overlap that is the hallmark of typical mixture modeling approaches, the multiscale clustering approach also results in partially overlapping clusters that share either common autocovariance parameters or residual covariance matrices but not both. The proposed approach ensures greater flexibility, since the clustering of the residual covariance does not directly interfere with the clustering for the autocovariance elements and vice-versa, which is expected to translate to increased accuracy. In contrast, a standard DP mixture specification, i.e. $(\Theta, \Sigma) \sim P_{\Theta, S}, P_{\Theta, S} \sim DP(\alpha P^*)$, yields clusters of replicated samples that share identical autocovariance *and* residual covariance parameters, which may become restrictive in larger dimensions since the number of parameters increase quadratically with D . The above discussions highlight the advantages of the multiscale clustering aspect and the associated partially overlapping clusters, which provide a central motivation for the development of the product of DP priors in this article.

While (3) provides a greater degree of flexibility in terms of accommodating heterogeneity compared to existing DP mixture approaches, there is further scope for generalizing this approach to accommodate additional heterogeneity in lag-specific and row-specific relationships. Such generalizations become particularly important when clusters of samples tend to share common autocovariance elements for some but not all lags or have identical elements for only a subset of rows/nodes in the autocovariance matrices. For example, the latter scenario arises when the effective clustering for the autocovariance elements is confined to a subset of rows in the matrix A , with the remaining rows being irrelevant with respect to clustering. Such aspects are routinely encountered in high-dimensional clustering problems

(Agrawal et al., 2005), including in our motivating HCP application (see Section 5). We now generalize the PDPM-VAR method below to account for such heterogeneous settings.

Generalization across lags: For the first extension, we specify independent DP priors for the autocovariance matrices at each lag, which results in lag-specific clustering as follows:

$$\text{vec}(A_k) \stackrel{\text{indep}}{\sim} P_{\Theta_k}, \quad P_{\Theta_k} \sim DP(\alpha_{1k} P_{1k}^*), \quad \Sigma \sim P_{\mathcal{S}}, \quad P_{\mathcal{S}} \sim DP(\alpha_2 P_2^*), \quad k = 1, \dots, K, \quad (5)$$

where P_{Θ_k} denotes the unknown density for $\text{vec}(A_k)$ that is modeled under a DP prior with base measure P_{1k}^* and precision parameter α_{1k} ($k = 1, \dots, K$), and the prior on the residual covariance parameters is defined similarly to (3), but with the understanding that α_2 and P_2^* in the DP priors in (5) and (3) are allowed to be distinct. The resulting product of DP priors in (5) may be expressed as $\Pi^*(\Theta, \Sigma) = P_{\mathcal{S}}(\Sigma) \times \prod_{k=1}^K P_{\Theta_k}(A_k)$. As under the PDPM-VAR, specification (5) induces a prior on the space of densities \mathcal{F} via

$$f_P(X) = \sum_{h_{11}=1}^{\infty} \dots \sum_{h_{1K}=1}^{\infty} \sum_{h_{\sigma}=1}^{\infty} \pi_{\sigma, h_{\sigma}} \left(\prod_{k=1}^K \pi_{k, h_{1k}} \right) \prod_{t=1}^T \phi_{\Sigma_{h_{\sigma}}} \left(\mathbf{x}_t - \sum_{k=1}^{\min\{t-1, K\}} A_{k, h_{1k}} \mathbf{x}_{t-k} \right), \quad (6)$$

where $\pi_{k, h_{1k}} = \nu_{k, h_{1k}} \prod_{l_{k, 1k} < h_{k, 1k}} (1 - \nu_{k, l_{1k}})$ ($k = 1, \dots, K$), $\pi_{\sigma, h_{\sigma}} = \nu_{\sigma, h_{\sigma}} \prod_{l_2 < h_{\sigma}} (1 - \nu_{\sigma, l_2})$ and $\nu_{k, h_{1k}} \sim Be(1, \alpha_{1k})$, $\nu_{\sigma, h_{\sigma}} \sim Be(1, \alpha_2)$, and further $\text{vec}(A_{k, h_{1k}}) \sim P_{1k}^*$, $\Sigma_{h_{\sigma}} \sim P_2^*$ for $k = 1, \dots, K$, using the stick-breaking construction in Sethuraman (1994). We denote the model under (1) and (5) as the lag-generalized product of DP mixture of VAR (lgPDPM-VAR) model and note that this model reduces to the PDPM-VAR for lag 1 models.

Generalization across autocovariance rows: It is also possible to generalize the PDPM-VAR model in (3) in an alternative manner that relaxes the restriction to have fully identical autocovariance matrices for all samples within a given autocovariance cluster. In particular, this approach specifies independent priors on the VAR model parameters corresponding to each row of the autocovariance matrices, which results in row-specific clustering patterns.

In particular, denote $A_{k,d'\bullet}$ as the d' -th row of A_k and consider the following specification

$$\text{vec}\{A'_{1,d'\bullet}, \dots, A'_{K,d'\bullet}\} \stackrel{\text{indep}}{\sim} P_{\Theta_{d'}}, \quad P_{\Theta_{d'}} \sim DP(\alpha_{d'}^* P_{1d'}^{**}), \quad \Sigma \sim P_S, \quad P_S \sim DP(\alpha_2 P_2^*), \quad d' = 1, \dots, D, \quad (7)$$

where A' denotes the transpose of A , and the row-specific priors $P_{\Theta_{d'}}(\text{vec}\{A'_{1,d'\bullet}, \dots, A'_{K,d'\bullet}\})$ are specified independently for each row and jointly across lags. The product of DP prior in (7) is expressed as $\Pi^*(\Theta, \Sigma) = P_S(\Sigma) \times \prod_{d'=1}^D P_{\Theta_{d'}}(\text{vec}\{A'_{1,d'\bullet}, \dots, A'_{K,d'\bullet}\})$, and results in the row-generalized PDPM-VAR (rgPDPM-VAR) model that induces priors on \mathcal{F} via

$$f_P(X) = \sum_{h_{1,1}=1}^{\infty} \dots \sum_{h_{1,D}=1}^{\infty} \sum_{h_{\sigma}=1}^{\infty} (\pi_{\sigma, h_{\sigma}} \prod_{d'=1}^D \pi_{d', h_{1d'}}^*) \prod_{t=1}^T \phi_{\Sigma_{h_{\sigma}}}(\mathbf{x}_t - \sum_{k=1}^{\min\{t-1, K\}} A_{k, h_{11}, \dots, h_{1D}} \mathbf{x}_{t-k}), \quad (8)$$

where $A_{k, h_{11}, \dots, h_{1D}}$ denotes the autocovariance matrix at lag k that assigns the $h_{1d'}$ -th mixture component to the d' -th row with prior probability $\pi_{d', h_{1d'}}^* = \nu_{d', h_{1d'}}^* \prod_{l_{1d'} < h_{1d'}} (1 - \nu_{l_{1d'}}^*)$,

with $\nu_{d', h_{1d'}}^* \sim Be(1, \alpha_{d'}^*)$ and $\text{vec}\{A'_{1,d'\bullet, h_{1,d'}}, \dots, A'_{K,d'\bullet, h_{1,d'}}\} \stackrel{\text{indep}}{\sim} P_{1d'}^{**}$ where $A_{k, d'\bullet, h_{1,d'}}$ denotes the d' -th row for the matrix A_k that takes values from the $h_{1,d'}$ -th mixture component.

Further, $\Sigma_{h_{\sigma}} \sim P_2^*$ with prior probability $\pi_{\sigma, h_{\sigma}} = \nu_{\sigma, h_{\sigma}} \prod_{l_2 < h_{\sigma}} (1 - \nu_{\sigma, l_2})$ and $\nu_{\sigma, h_{\sigma}} \sim Be(1, \alpha_2)$.

In the scenario when multiple rows have identical clustering configurations, the rgPDPM-VAR model is able to recover clusters of samples that share identical autocovariance elements corresponding to a subset of nodes only, with possible within-cluster variations corresponding to the remaining autocovariance rows. We note that for our motivating neuroimaging applications, this scenario translates to identical effective connectivity corresponding to a subset of brain regions within a autocovariance cluster, while the remaining brain regions are allowed to exhibit varying connectivity profiles within this cluster. By allowing a collection of partially overlapping autocovariance clusters with varying degrees of overlap, the rgPDPM-VAR approach results in a more complete characterization of heterogeneity compared to the PDPM-VAR. Additional generalizations are also possible; for

example, one may extend specification (7) to impose row- and lag-specific priors. However, such extensions may result in a rapid rise in parameters that presents potential computational issues. Hence, we do not consider such generalizations further in this article and restrict our attention to the PDPM-VAR, lgPDPM-VAR and rgPDPM-VAR variants.

2.2 Theoretical Properties

Notations and Definitions: In this section we will establish posterior consistency properties of the proposed product of DP mixture of VAR models. We will assume that the $D \times T$ data matrices X_1, \dots, X_n , are i.i.d. under some true density $f_0 \in \mathcal{F}$. We will study the convergence of the posterior around this true density with respect to the product measure F_0^n associated with f_0 as n grows to ∞ , under some reasonable regularity conditions on f_0 and the conditions on the tail behavior of the base measures of the DP priors. We note that our theoretical treatment does not require f_0 to correspond to a VAR model, which makes the proposed approach more robust to mis-specification. The convergence in the space of densities \mathcal{F} is evaluated in terms of the Hellinger distance defined as $d(f, g) = [\int (\sqrt{f} - \sqrt{g})^2]^{1/2}$, as well as the L_1 metric defined as $\|f - g\|_1 = \int |f - g|$.

Some additional notations are provided below. Denote the Euclidean norm for a vector as $\|\cdot\|$, and denote the spectral norm of a matrix as $\|\cdot\|_2$. Further, denote the eigenvalues of a $D \times D$ positive definite matrix Σ in decreasing order as $\lambda_1(\Sigma) \geq \dots \geq \lambda_D(\Sigma)$. Let $a \lesssim b$ imply that a is less than b upto a constant, and $\lfloor \cdot \rfloor$ denote the floor operator. Denote the Kullback-Leibler (KL) divergence between densities $f, g \in \mathcal{F}$ as $KL(f, g) = \int \log(f/g)f$. We denote the entropy of a space of densities $\mathcal{G} \subset \mathcal{F}$ as $N(\epsilon, \mathcal{G}, d)$, which is defined (in terms of the metric d) as the minimum integer N for which there exists densities $f_1, \dots, f_N \in \mathcal{F}$ satisfying $\mathcal{G} \subset \bigcup_{j=1}^N \{f : d(f, f_j) < \epsilon\}$. Denote the set of natural numbers as \mathbb{N} .

Throughout the article, we will assume the following reasonable regularity conditions on f_0 , which are based on standard assumptions made in multivariate density estimation

literature. Let $f_0(\mathbf{x}_t \mid X_{1:(t-1)})$ denote the true conditional density of \mathbf{x}_t given data at previous time scans. Consider the following assumptions.

- (A0) The form of the true density satisfies $f_0(X) = \{ \prod_{t=1}^T f(\mathbf{x}_t \mid \mathbf{x}_{t-1}, \dots, \mathbf{x}_1) \} = \{ \prod_{t=1}^T f(\mathbf{x}_t \mid X_{1:(t-1)}) \}$, for all $X \in \mathbb{R}^{D \times T}$.
- (A1) $0 < f_0(X) < M$ for some constant M and for all $X \in \mathbb{R}^{D \times T}$.
- (A2) $|\int f_0(\mathbf{x}_t \mid X_{1:(t-1)}) \log(f_0(\mathbf{x}_t \mid X_{1:(t-1)})) d\mathbf{x}_t| < \infty$, point-wise for $X_{1:(t-1)}$ for all t .
- (A3) For all t and some $\delta > 0$, $\int f_0(\mathbf{x}_t \mid X_{1:(t-1)}) \log\left(\frac{f_0(\mathbf{x}_t \mid X_{1:(t-1)})}{\phi_\delta^*(\mathbf{x}_t \mid X_{1:(t-1)})}\right) d\mathbf{x}_t < \infty$, where $\phi_\delta^*(\mathbf{x}_t \mid X_{1:(t-1)}) = \inf_{\|\mathbf{r} - \mathbf{x}_t\| < \delta} f_0(\mathbf{r} \mid X_{1:(t-1)})$, point-wise for $X_{1:(t-1)}$.
- (A4) For all t and some $\eta > 0$, $\int \|\mathbf{x}_t\|^{2(1+\eta)} f_0(\mathbf{x}_t \mid X_{1:(t-1)}) d\mathbf{x}_t < \infty$, point-wise for $X_{1:(t-1)}$.

Condition (A0) expresses the true density as a product of conditional densities, subject to a known K , and further assumes that the true conditional density only depends on $\mathbf{x}_{t-1}, \mathbf{x}_{t-2}, \dots, \mathbf{x}_{t-K}$, when $t > K$ and depends on $\mathbf{x}_{t-1}, \mathbf{x}_{t-2}, \dots, \mathbf{x}_1$ for $t \leq K$. Condition (A1) assumes that the true density is bounded. Assumptions (A2)-(A4) impose regularity conditions on the conditional densities that are similar to standard assumptions made in nonparametric Bayesian literature for marginal densities (Wu and Ghosal, 2008). In the special case when the true density corresponds to a VAR structure, (A0)-(A4) would imply (among other things) that the true VAR parameters are well-behaved and satisfy stability conditions so that the true density does not blow up to ∞ or attenuate to zero.

The following Theorem formally states the result on positive prior support under the above assumptions. The proof is provided in the Supplementary Materials and uses key results in Wu and Ghosal (2008) for multivariate density estimation under DP mixtures.

Theorem 1: *Suppose assumptions (A0) – (A4) are satisfied. Then the product of DP mixture priors Π specified in (3), (5), and (7) satisfies the Kullback-Leibler property, i.e. $\Pi\left(f \in \mathcal{F} : \int \log(f_0/f) f_0 \leq \eta^*\right) \geq 0$, for any $\eta^* > 0$.*

Remark 1: Theorem 1 provides weak consistency guarantees by establishing positive prior

support for arbitrarily small Kullback-Leibler neighborhoods of f_0 , as per Schwartz (1965).

Although weak consistency suggests the ability of the proposed method to accurately recover the true density, in many cases Kullback-Leibler neighborhoods contain densities that may show non-negligible deviations from f_0 . Hence it is of interest to investigate strong consistency for the proposed approach, which renders the desirable feature that the posterior distribution concentrates in arbitrarily small L_1 neighborhoods of the true density. In order to establish the strong consistency property for non-compact space of densities \mathcal{F} , it is imperative to carefully design sieves \mathcal{F}_n that are compact subsets of \mathcal{F} but that grow with n to eventually cover all of \mathcal{F} as $n \rightarrow \infty$. A careful choice for the sieve needs to be made to ensure that the metric entropy grows slowly with n , while the prior probability of the complement of \mathcal{F}_n (denoted as \mathcal{F}_n^c) decreases exponentially fast, such that a sufficient summability condition holds which guarantees strong consistency as per ideas in Theorem 5 of Ghosal and Van Der Vaart (2007). The following result, which is similar to Theorem 1 in Canale and De Blasi (2017) for multivariate density estimation and is stated here for brevity, captures the sufficient conditions characterizing the sieves.

Theorem 2: *Consider sieves $\mathcal{F}_n \subset \mathcal{F}$ with $\mathcal{F}_n \uparrow \mathcal{F}$ as $n \rightarrow \infty$, where $\mathcal{F}_n = \cup_j \mathcal{F}_{n,j}$, such that (2A) $\Pi(\mathcal{F}_n^c) \lesssim \exp^{-bn}$ for $b > 0$; and (2B) $\sum_j \sqrt{N(2\epsilon, \mathcal{F}_{n,j}, d)} \sqrt{\Pi(\mathcal{F}_{n,j})} \exp^{-(4-c)n\epsilon^2} \rightarrow 0$, for $c, \epsilon > 0$. Then $\Pi(f : d(f_0, f) > 8\epsilon \mid X^{(1)}, \dots, X^{(n)}) \rightarrow 0$ in F_0^n -probability for any f_0 in the weak support of Π under the PDPM-VAR, lgPDPM-VAR, and rg-PDPM-VAR.*

In Theorem 2, condition (2A) suggests that the sieve should grow with the sample size such that only small neighborhoods with exponentially small prior probabilities are excluded. On the other hand, condition (2B) reflects the summability condition that involves smaller subsets $\mathcal{F}_{n,j}$ that cover the sieve \mathcal{F}_n under the union operation. It places constraints on the growth rate of the metric entropy in a manner that the weighted sum

of the square root of metric entropy of $\mathcal{F}_{n,j}$ (weighted by the corresponding square root of prior probabilities) go towards zero with increasing n . In practice, it is not straightforward to construct such sieves since the metric entropy depends on a number of terms including the sample size n , dimension D , as well as T (see Theorem 3). It turns out that one can apply a stick-breaking representation to construct appropriate sieves inspired by the ideas implemented in Shen et al. (2013) for multivariate density estimation. However, it is not possible to directly adapt the sieves used in non-parametric Bayesian univariate and multivariate density estimation to our settings of interest that involve matrix-variate data modeled under a VAR framework and under a product of DP priors.

The sieves corresponding to our models are constructed so as to allow the norm of the elements in the autocovariance matrices, as well as the condition number of the residual covariance matrices, to increase with sample size at an appropriate rate that satisfies the conditions in Theorem 2. We note that the condition number of a matrix frequently appears in the random matrix literature (Edelman, 1988) and is defined as the ratio of the largest to the smallest eigen values, i.e. $\lambda_1(\Sigma)/\lambda_D(\Sigma) = \lambda_1(\Sigma^{-1})/\lambda_D(\Sigma^{-1})$. For our purposes, we construct the following sieves corresponding to the PDPM-VAR model in (1) and (3):

$$\begin{aligned} \mathcal{F}_n &= \left\{ f_p : P = \sum_{h_1 \geq 1} \sum_{h_\sigma \geq 1} \pi_{h_1} \pi_{\sigma, h_\sigma} \delta_{\Theta_{h_1}, \Sigma_{h_\sigma}} : \sum_{h_1 > H_n} \pi_{h_1} < \epsilon_1, \sum_{h_\sigma > H_n} \pi_{\sigma, h_\sigma} < \epsilon_2, \text{ and for} \right. \\ &\quad \left. h_\sigma \leq H_n, \underline{\sigma}_n^2 \leq \lambda_{D, \Sigma_{h_\sigma}} \leq \lambda_{1, h_\sigma} \leq \underline{\sigma}_n^2 (1 + \epsilon/\sqrt{D})^{M_n}, 1 < \frac{\lambda_{1, h_\sigma}}{\lambda_{D, h_\sigma}} \leq n^{H_n} \right\}, \\ \mathcal{F}_{n, \mathbf{j1}} &= \left\{ f_p \in \mathcal{F}_n : \text{for } h_1, h_\sigma \leq H_n, \underline{a}_{h_1, j} \leq \|\text{vec}(A_{k, h_1})\| \leq \bar{a}_{h_1, j} \ \forall k, \underline{u}_{h_\sigma, l} \leq \frac{\lambda_{1, h_\sigma}}{\lambda_{D, h_\sigma}} \leq u_{h_\sigma, l} \right\} \quad (9) \end{aligned}$$

where $\delta(\cdot)$ denotes the Dirac delta function, $\lambda_{d', \Sigma_{h_\sigma}}$ denotes $\lambda_{d'}(\Sigma_{h_\sigma})$, $d' = 1, \dots, D$, i.e. the D eigen values corresponding to Σ_{h_σ} , j, l are integers that are $\leq H_n$ for a given n , the sequences $\{H_n\}, \{M_n\}, \{\underline{\sigma}_n\} \{\underline{a}_{h_1, j}\}, \{\bar{a}_{h_1, j}\}, \{\underline{u}_{h_\sigma, j}\}, \{\bar{u}_{h_\sigma, j}\}$ grow to ∞ with n and are chosen appropriately such that $\mathcal{F}_n \subset \bigcup_{\mathbf{j1}} \mathcal{F}_{n, \mathbf{j1}}$, and further, $\mathcal{F}_n \uparrow \mathcal{F}$ as $n \rightarrow \infty$. The sieves

for the lgPDPM-VAR model in (1) and (5) are constructed similarly as:

$$\begin{aligned}
\mathcal{F}_n = & \left\{ f_p : P = \sum_{h_{11}=1}^{\infty} \dots \sum_{h_{1K}=1}^{\infty} \sum_{h_{\sigma}=1}^{\infty} \pi_{\sigma, h_{\sigma}} \left(\prod_{k=1}^K \pi_{k, h_{1k}} \right) \delta_{\Theta_{h_{1k}}, \Sigma_{h_{\sigma}}} : \sum_{h_{1,1k} > H_n} \pi_{k, h_{1k}} < \epsilon_1, \forall k = 1, \dots, K, \right. \\
& \left. \sum_{h_{\sigma} > H_n} \pi_{\sigma, h_{\sigma}} < \epsilon_2, \text{ and for } h_{\sigma} \leq H_n, \underline{\sigma}_n^2 \leq \lambda_D(\Sigma_{h_{\sigma}}) \leq \lambda_1(\Sigma_{h_{\sigma}}) \leq \underline{\sigma}_n^2 (1 + \epsilon/\sqrt{D})^{M_n}, 1 < \frac{\lambda_{1, h_{\sigma}}}{\lambda_{D, h_{\sigma}}} \leq n^{H_n} \right\}, \\
\mathcal{F}_{n, \mathbf{jl}} = & \left\{ f_p \in \mathcal{F}_n : \underline{a}_{h_{1k}, j} \leq \| \text{vec}(A_{k, h_{1k}}) \| \leq \bar{a}_{h_{1k}, j} \text{ for all } h_{1k} \leq H_n, \underline{u}_{h_{\sigma}, l} \leq \frac{\lambda_{1, h_{\sigma}}}{\lambda_{D, h_{\sigma}}} \leq u_{h_{\sigma}, l}, h_{\sigma} \leq H_n \right\}, \\
(10) \quad &
\end{aligned}$$

and the sieves corresponding to rgPDPM-VAR in (1) and (7) are constructed as:

$$\begin{aligned}
\mathcal{F}_n = & \left\{ f_p : P = \sum_{h_{1,1}=1}^{\infty} \dots \sum_{h_{1,D}=1}^{\infty} \sum_{h_{\sigma}=1}^{\infty} \left(\pi_{\sigma, h_{\sigma}} \prod_{d'=1}^D \pi_{d', h_{1d'}}^* \right) \delta_{\Theta_{h_{1d'}}, \Sigma_{h_{\sigma}}} : \sum_{h_{1d'} > H_n} \pi_{d', h_{1d'}}^* < \epsilon_1, \forall d' \leq D, \right. \\
& \left. \sum_{h_{\sigma} > H_n} \pi_{\sigma, h_{\sigma}} < \epsilon_2, \text{ and for } h_{\sigma} \leq H_n, \underline{\sigma}_n^2 \leq \lambda_{D, h_{\sigma}} \leq \lambda_{1, h_{\sigma}} \leq \underline{\sigma}_n^2 (1 + \epsilon/\sqrt{D})^{M_n}, 1 < \frac{\lambda_{1, h_{\sigma}}}{\lambda_{D, h_{\sigma}}} \leq n^{H_n} \right\}, \\
\mathcal{F}_{n, \mathbf{jl}} = & \left\{ f_p \in \mathcal{F}_n : \underline{a}_{h_{1d'}, j} \leq \| \text{vec}(A_{k, d' \bullet, h_{1, d'}}) \| \leq \bar{a}_{h_{1d'}, j} \text{ for } h_{11}, \dots, h_{1D} \leq H_n, \right. \\
& \left. \text{and } d' = 1, \dots, D, \text{ and } \underline{u}_{h_{\sigma}, l} \leq \frac{\lambda_{1, h_{\sigma}}}{\lambda_{D, h_{\sigma}}} \leq u_{h_{\sigma}, l}, \text{ for } h_{\sigma} \leq H_n \right\}, \\
(11) \quad &
\end{aligned}$$

where $\mathcal{F}_n \subset \cup_{\mathbf{jl}} \mathcal{F}_{n, \mathbf{jl}}$ and $\mathcal{F}_n \uparrow \mathcal{F}$ as $n \rightarrow \infty$, and it is understood that the sequences $\{H_n\}, \{M_n\}, \{\underline{\sigma}_n\}, \{\underline{a}_{h_{1j}}\}, \{\bar{a}_{h_{1j}}\}, \{\underline{u}_{h_{\sigma}, l}\}, \{u_{h_{\sigma}, l}\}$ are chosen appropriately and can be specific to sieves corresponding to PDPM-VAR, lgPDPM-VAR or rgPDPM-VAR. The following results establish entropy bounds that are vital to establishing strong consistency.

Theorem 3: *The entropy bound for sieves (9) satisfies $N(\epsilon, \mathcal{F}_{n, \mathbf{jl}}, \|\cdot\|_1) \lesssim \left(\frac{M^D}{\epsilon^{-C_1}} \right)^{H_n} \times \prod_{h_{\sigma} \leq H_n} \left\{ \frac{2Du_{h_{\sigma}, l}}{\epsilon^2} \right\}^{D(D-1)/2} \times \prod_{h_1 \leq H_n} \left\{ \left(\frac{C_{h_{1j}, h_{\sigma}, l}^* \bar{a}_{h_{1j}}}{\underline{\sigma}_n \epsilon} + 1 \right)^{D^2} - \left(\frac{C_{h_{1j}, h_{\sigma}, l}^* a_{h_{1j}}}{\underline{\sigma}_n \epsilon} - 1 \right)^{D^2} \right\}^K$, where $C_1 > 0$ and $C_{h_{1j}, h_{\sigma}, l}^* > 0$ that depends on (D, t, K) .*

Corollary 1: *The entropy satisfies $N(\epsilon, \mathcal{F}_{n, \mathbf{jl}}, \|\cdot\|_1) \lesssim \left(\frac{M^D}{\epsilon^{-C_1}} \right)^{H_n} \times \prod_{h_{\sigma} \leq H_n} \left\{ \frac{2Du_{h_{\sigma}, l}}{\epsilon^2} \right\}^{D(D-1)/2} \times$*

\mathcal{K}^* , where $\mathcal{K}^* = \prod_{h_{11} \leq H_n} \cdots \prod_{h_{1K} \leq H_n} \left\{ \left(\frac{C_{h_{1,j}, h_{\sigma,l}}^{**} \bar{a}_{h_{1k},j}}{\underline{\sigma}_n \epsilon} + 1 \right)^{D^2} - \left(\frac{C_{h_{1,j}, h_{\sigma,l}}^{**} a_{h_{1k},j}}{\underline{\sigma}_n \epsilon} - 1 \right)^{D^2} \right\}$ for sieves (10), and $\mathcal{K}^* = \prod_{h_{11} \leq H_n} \cdots \prod_{h_{1D} \leq H_n} \left\{ \left(\frac{\tilde{C}_{h_{1,j}, h_{\sigma,l}}^* \bar{a}_{h_{1d'},j}}{\underline{\sigma}_n \epsilon_2} + 1 \right)^D - \left(\frac{\tilde{C}_{h_{1,j}, h_{\sigma,l}}^* a_{h_{1d'},j}}{\underline{\sigma}_n \epsilon_2} - 1 \right)^D \right\}^K$ corresponding to sieves (11), with $C_1 > 0$ and $C_{h_{1,j}, h_{\sigma,l}}^{**}, \tilde{C}_{h_{1,j}, h_{\sigma,l}}^* > 0$ depending on (D, t, K) .

Remark 1: The constant C_1 in the entropy bounds is understood to be different corresponding to sieves in (9), (10), and (11).

Having established the entropy bounds, the next step is to propose sensible base measures that satisfies the above entropy bounds and also facilitate posterior computations. These base measures are characterized via conditions on the tail probabilities that are elaborated below, and include some commonly used choices as discussed in the sequel.

(B1) The base measures corresponding to P_S in (3), (5) and (7) satisfy $P_2^*(\lambda_1(\Sigma_{h_\sigma}^{-1}) > x^*) \lesssim \exp(-c_1(x^*)^{c_2})$, $P_2^*(\lambda_D(\Sigma_{h_\sigma}^{-1}) < 1/x^*) \lesssim (x^*)^{-c_3}$, $P_2^*(\frac{\lambda_1(\Sigma_{h_\sigma}^{-1})}{\lambda_D(\Sigma_{h_\sigma}^{-1})} > x^*) \lesssim (x^*)^{-\kappa}$, for some constants c_1, c_2, c_3, κ , and corresponding to the cluster h_σ .

(B2) The base measure corresponding to P_Θ specifies independence across lags, and satisfies the following tail conditions: (i) under PDPM-VAR, $P_1^*(\|vec(A_{k,h_1})\| > x^*) \lesssim (x^*)^{-2(r+1)}$ for cluster h_1 ; (ii) under lgPDPM-VAR, $P_{1k}^*(\|vec(A_{k,h_{1k}})\| > x^*) \lesssim (x^*)^{-2(r+1)}$ for cluster h_{1k} ; and (iii) under rgPDPM-VAR, $P_{1d'}^*(\|vec\{A'_{1,d',\bullet,h_{1,d'}}, \dots, A'_{K,d',\bullet,h_{1,d'}}\}\| > x^*) \lesssim (x^*)^{-2(r^*+1)}$ corresponding to cluster $h_{1d'}$, for some constants $r, r^* > 0$, and $d' = 1, \dots, D$.

The above conditions on the base measures are very reasonable and hold for commonly used distributions on autocovariance matrices (such as Gaussian and Laplace), as well as inverse-Wishart distribution corresponding to P_2^* . In addition, it is also possible to specify low rank structures on the residual covariance along with appropriate priors that satisfy the tail conditions in (B1). Such low rank representations are routinely used for dimension reduction in the factor model literature (Ghosh and Dunson, 2009) and are

particularly useful for developing scalable posterior computation strategies for the proposed VAR models. Denote $\mathcal{A}_{d',h_{1,d'}} = \text{vec}\{A'_{1,d' \bullet, h_{1,d'}}, \dots, A'_{K,d' \bullet, h_{1,d'}}\}$ and let DE denote a double exponential prior. Lemmas 1-2 formalizes the above discussions on the base measures.

Lemma 1: *Condition (B2) holds when $P_1^*(\text{vec}(A_{k,h_1}))$ is specified as $N_{D^2}(\text{vec}(A_k); \boldsymbol{\mu}, \Lambda)$ with $\Lambda \sim IW(\Lambda_0, \nu_\lambda)$ corresponding to PDPM-VAR, and for a similar choice of $P_{1k}^*(\text{vec}(A_{k,h_{1k}}))$ under lg-PDPM-VAR. It is also satisfied when $P_{1d'}^{**}(\mathcal{A}_{d',h_{1,d'}}) = \prod_{k=1}^K N_D(A_{k,d' \bullet, h_{1,d'}}; \boldsymbol{\mu}, \Lambda_{d'})$, $\Lambda_{d'} \sim IW(\Lambda_{0d'}, \nu_{\lambda,d'})$, under rgPDPM-VAR. Further, (B2) also holds if the above base measures are changed to a product of independent $DE(\lambda)$ priors with suitably large λ .*

Lemma 2: *Condition (B1) holds when for cluster h_σ , $P_2^*(\Sigma_{h_\sigma}) = IW(\Sigma_{h_\sigma}; \Sigma_0, \nu_\sigma)$, as well as under the low rank representation $\Sigma_{h_\sigma} = \Gamma_{h_\sigma} \Gamma_{h_\sigma}^T + \Omega_{h_\sigma}$ where Γ_{h_σ} is $D \times B$ and $\Omega_{h_\sigma} = \text{diag}(\sigma_{1,h_\sigma}^2, \dots, \sigma_{D,h_\sigma}^2)$, and $P_2^*(\Sigma_{h_\sigma}) = \left\{ \prod_{d'=1}^D \prod_{m'=1}^B N(\gamma_{d'm',h_\sigma}; 0, 1) \right\} \left\{ \prod_{j=1}^D Ga(\sigma_{j,h_\sigma}^2; a_\sigma, b_\sigma) \right\}$.*

The proof of Lemma 1 is provided in the Supplementary Materials, while that of Lemma 2 follows directly from Corollaries 1 and 2 in Canale and De Blasi (2017). We note that $B << D$ in Lemma 2 ensures a reduced rank structure on the residual covariance matrix.

One can now use the entropy bounds derived in Theorem 3 and Corollaries 1-2 along with tail conditions in (B1)-(B2) to establish our strong consistency under a broad class of base measures, by applying Theorem 2. Our strong consistency result is stated below.

Theorem 4: *Suppose Theorem 1 holds, and (B1)-(B2) are satisfied. Then for suitably large constants r, r^*, κ , the posterior distribution corresponding to the PDPM-VAR, lgPDPM-VAR and rgPDPM-VAR are strongly consistent at f_0 under suitable sequences $\{H_n\}, \{M_n\}, \{\underline{\sigma}_n\} \{\underline{a}_{h_1,j}\}, \{\bar{a}_{h_1,j}\}, \{\underline{u}_{h_\sigma,j}\}, \{\underline{u}_{h_\sigma,j}\}$ in the sieves (9), (10), and (11).*

Remark 2: In mathematical terms, strong posterior consistency can be written as $\Pi(\{f : d(f, f_0) > \epsilon_f\} \mid X_1, \dots, X_n) \rightarrow 0$ as $n \rightarrow \infty$ in F_0^n probability for any $\epsilon_f > 0$ and with $d(\cdot)$ denoting the Hellinger or L_1 metric.

3 Posterior Computation

We utilize block Gibbs samplers to fit all proposed models. Our approach alternates between sampling parameters related to the autocovariance matrices and the residual covariance matrix. For all models, we update the autocovariance parameters row-wise for one outcome at a time. In order to scale up the implementation of the proposed method to high dimensional applications, we use a reduced rank factor model representation for the residual covariance matrix in our implementation, which provides a desired balance between computational scalability and theoretical flexibility. In particular, such a low rank structure on the residual covariance does not adversely impact the accuracy of parameter estimates compared to an unstructured covariance matrix, in our experience involving extensive numerical experiments with true unstructured residual covariances. Further, it is considerably more flexible and results in greater accuracy compared to a diagonal residual covariance that is routinely used in VAR literature (Kook et al., 2021) but may be restrictive in fMRI applications which have known functional connectivity structures. In particular, we specify $\Sigma_i = \boldsymbol{\Gamma}_i \boldsymbol{\Gamma}_i' + \boldsymbol{\Psi}_i$, where $\boldsymbol{\Gamma}_i$ is a $D \times B$ factor loadings matrix with $B(< D)$ factors, and $\boldsymbol{\Psi}_i$ is $\text{diag}\{\sigma_{i,1}^2, \dots, \sigma_{i,D}^2\}$. To facilitate posterior computation, we use the following equivalent augmented representation:

$$\mathbf{x}_{i,t} = \sum_{k=1}^{\min\{t-1, K\}} A_{ik} \mathbf{x}_{i,t-k} + \boldsymbol{\Gamma}_i \boldsymbol{\eta}_{i,t} + \boldsymbol{\epsilon}_{i,t}^*, \quad \boldsymbol{\epsilon}_{i,t}^* \sim N(0, \boldsymbol{\Psi}_i), \quad i = 1, \dots, n, \quad t = 1, \dots, T_i, \quad (12)$$

where $\boldsymbol{\eta}$ represents the latent factors that can be marginalized out to recover the VAR model $\mathbf{x}_{i,t} = \sum_{k=1}^{\min\{t-1, K\}} A_{ik} \mathbf{x}_{i,t-k} + \boldsymbol{\epsilon}_{i,t}$, $\boldsymbol{\epsilon}_{i,t} \sim N(0, \boldsymbol{\Gamma}_i \boldsymbol{\Gamma}_i' + \boldsymbol{\Psi}_i)$. The computationally efficient fully Gibbs sampler for the proposed approach is described in detail in the Supplementary Materials, and includes expressions for posterior distributions for sampling all the model parameters. We note that it is straightforward to generalize the Gibbs sampler to include an unstructured residual covariance that does not respect a reduced rank representation.

4 Simulation Studies

We compared the performance under the proposed approaches to a state-of-the-art single-subject VAR approach, as well as an ad-hoc clustering extension of the single subject VAR model that is able to borrow information across samples. We generated data for $n = 100, 200$, $D = 40, 100$, $T_i \in \{250, 350\}$, and different levels of sparsity within the autocovariance matrices were considered (75% and 90%). For each data generation setting we generate 25 simulation replicates, and for all settings the true VAR model involved $K = 2$ lags. We consider four settings for generating the subject-level autocovariance matrices that differ with respect to the clustering structure. Settings 1-3 represent the PDPM-VAR, lgPDPM-VAR and rgPDPM-VAR scenarios respectively, while Setting 4 represents a more heterogeneous setting that is obtained via introducing additional random noise to the autocovariance elements generated under Setting 3. For Setting 1, we use 3 autocovariance clusters, for Setting 2 we use 3 clusters for lag 1 and 2 clusters for lag 2, and for Settings 3-4 we vary the true number of clusters randomly (between 2 – 5) across rows of the autocovariance matrix, and the elements of these matrices are generated randomly in order to ensure a stable time series. In Setting 3, subjects within a cluster share the exact same elements for the corresponding rows of the autocovariance matrix, whereas in Setting 4 the subject-level rows of the autocovariance matrix within a cluster are random deviations from a shared mean row. Each cluster's residual covariance matrix was generated from an Inverse Wishart distribution with D degrees of freedom and diagonal scale matrix with elements equal to $D/2$. Subject level time courses were obtained by starting with random values for the multivariate observation at the first time point, and subsequently generating future observations from the assumed true VAR model. For a subject, an additional 5 time scans were generated after the initial T_i observations to evaluate forecasting accuracy.

4.1 Approaches and Performance Metrics

We compare the proposed approaches to the single subject Bayesian VAR (SS-VAR) model developed in Ghosh et al. (2018), which separately models the time courses for each subject. We also consider a two-stage clustering extension of this method, where we first estimated subject specific autocovariance and residual covariances under the single VAR approach by Ghosh et al. (2018) and then applied the k-means clustering separately to the vectorized autocovariance and residual covariance matrix estimates. We choose the number of clusters to maximize the silhouette score (Rousseeuw, 1987) and we then allocate each sample to one of the k clusters that is based on both the autocovariance terms and the residual covariance estimates from the initial SS-VAR fit. We subsequently concatenate the time courses across all subjects within the same cluster in order to borrow information within cluster, and finally re-fit the SS-VAR model to this concatenated data separately for each cluster. Since the true clustering structure was assumed to be unknown when fitting the model, it was not possible to compare the performance with existing multi-subject VAR modeling methods that assume known groupings (Chiang et al., 2017; Kook et al., 2021).

We evaluate performance in terms of (1) autocovariance estimation accuracy, (2) clustering accuracy, (3) feature selection for identifying structural zeros in the autocovariance matrices, and (4) forecasting accuracy. Following Ghosh et al. (2018), we measure estimation accuracy using the relative L2 error of the estimates to the true estimates. Clustering accuracy is measured using the adjusted Rand index (Rand, 1971), which measures agreement between the assigned and true cluster labels, adjusted for chance agreement. Feature selection performance is evaluated via area under the receiver operating characteristic (RoC) curve and precision recall curve (PRC). To calculate both curves we considered a sequence of significance thresholds, and for each threshold, we examined the corresponding credible interval to infer the significance. The corresponding sequence of sensitivity versus

1-specificity values were plotted over varying thresholds in order to obtain the ROC curve, while the PRC was obtained by plotting the positive predictive value ($1 - FDR$) against sensitivity (FDR denotes the false discovery rate). Finally, forecasting accuracy is measured via the relative L2 error of the predicted time courses for time scans $T_i + 1, \dots, T_i + 5$.

4.2 Simulation Results

Simulation results are presented in Figures 1–2. Due to space constraints, we provide the simulation results for the most challenging case ($D = 100, T = 250$) at the 75% sparsity level here and present the other cases in the Supplementary Materials. Several general patterns are clear from the results. First, the clustering performance for the autocovariance depends heavily on the true clustering structure (Figure 1, Panel A), with the PDPM-VAR, lg-PDPMVAR, and rgPDPM-VAR generally outperforming the other approaches when the data is generated from Settings 1-3 respectively. However, the rgPDPM-VAR often has close to optimal clustering performance when the PDPM-VAR is the true model and it also performs the best for the heterogeneous Setting 4, which reflects the generalizability of this variant. Critically, when there are differences in clustering across the different outcomes corresponding to more heterogeneous scenarios (e.g. Settings 3-4), only the rgPDPM-VAR is able to achieve a good clustering score. Finally, across all settings, the SS-VAR with clustering has the worst performance, demonstrating that the ad hoc two-stage analysis procedure is not able to accurately pool information across subjects.

The areas under the ROC and PR curves (Figure 1, Panels C and D) illustrate a consistently superior feature selection performance under the three proposed variants compared to the single subject VAR model with and without clustering. As expected, the PDPM-VAR, lgPDPM-VAR and rgPDPM-VAR approaches have higher area under the ROC and PR curves when the data is generated from Settings 1-3 respectively. In addition, the rgPDPM-VAR often has comparable area under the curve with PDPM-VAR for $n = 200$

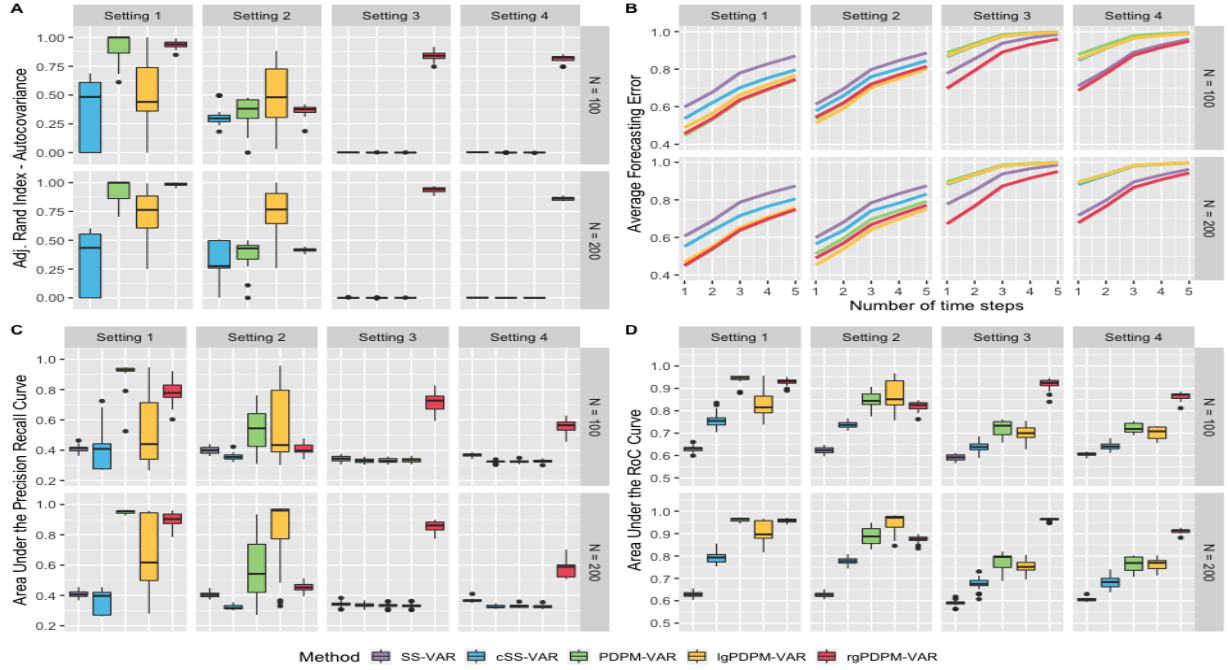


Figure 1: Simulation results for $D = 100$, $T = 250$ case with sparsity level 0.75. Panel A displays the adjusted Rand index for clustering the autocovariance. Panel B displays the forecasting error. Panels C and D display the area under the PR and RoC curves for identifying autocovariance non-zero elements.

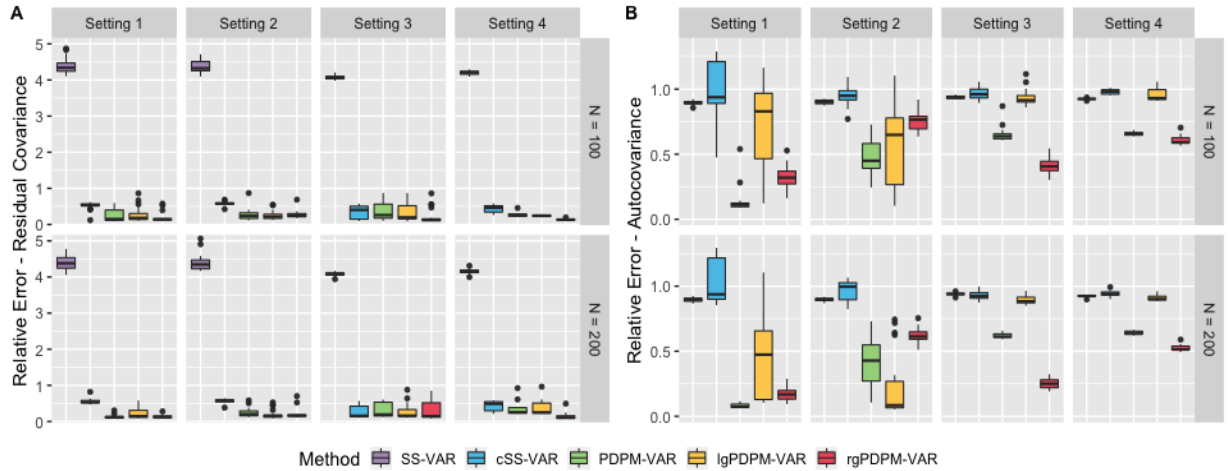


Figure 2: Relative L1 error for estimating the residual covariance (Panel A) and the subject-specific autocovariance matrices (Panel B) for $D = 100$, $T = 250$ case with sparsity level 0.75.

under Setting 1 and the best performance under the more heterogeneous Setting 4. These results imply the ability of rgPDPM-VAR to accurately identify the sparsity structure of the autocovariance with a low risk of false discoveries for data with unknown clustering.

When estimating the residual covariance matrices (Figure 2, Panel A), all three proposed approaches are able to heavily outperform the SS-VAR model. The performance under the three proposed approaches is generally comparable, with the rgPDPM-VAR outperforming the others in the more heterogeneous Settings 3 and 4. In addition, the SS-VAR approach with initial clustering has a higher relative error compared to the rgPDPM-VAR for the vast majority of cases, although it occasionally has a slightly improved performance in Setting 3. We conjecture that this is due to the assumed full rank structure for the residual covariance that is modeled via an inverse-Wishart distribution under the SS-VAR, which aligns with the true data generation scenario, in contrast to the assumed low-rank structure on the PDPM-VAR. Unfortunately, the SS-VAR approach with clustering has extremely poor performance in terms of autocovariance estimation (Figure 2, Panel B), while the PDPM-VAR, lgPDPM-VAR, and rgPDPM-VAR approaches typically have the lowest errors when the data is generated from Settings 1-3 respectively. The rgPDPM-VAR method also has the best autocovariance estimation performance under the more heterogeneous Setting 4.

Figure 1 Panel B displays the forecasting error for each of the autocovariance clustering setups, averaged over the sparsity level and the number of time points per subject. With the exception of Setting 2 where lgPDPM-VAR performs best, the rgPDPM-VAR approach has the best or close to optimal forecasting performance for other settings. Moreover, in the more heterogeneous Settings 3-4, the SS-VAR method with initial clustering has better forecasting accuracy compared to the PDPM-VAR and lgPDPM-VAR approaches, although it can not outperform the rgPDPM-VAR method. The relative forecasting performance levels off for greater than three time steps.

Synopsis of findings: Overall, the rgPDPM-VAR provides a desirable balance between model parsimony and accurate estimation and inference across various degrees of heterogeneity across samples. The advantages under the rgPDPM-VAR are most pronounced under the heterogeneous Settings 3 and 4, and it often has close to optimal performance in Setting 1 for larger n . This illustrates the advantages of pooling information across subjects, while accommodating varying levels of heterogeneity at the level of the rows of the autocovariance matrix. While the SS-VAR approach with ad-hoc clustering is also able to pool information, it is highly sensitive to the clustering accuracy in the first step, and it can not capture clustering uncertainty, resulting in inferior performance.

5 Analysis of Human Connectome Project Data

5.1 Analysis Description

We use the rgPDPM-VAR approach to investigate effective connectivity differences between individuals with high and low fluid intelligence (FI) using a subset of resting-state fMRI data from the Human Connectome Project. Preprocessing details for these data can be found in (Smith et al., 2013). We adopt the 360-region Glasser atlas for parcellation as in Akiki and Abdallah (2019), where each node has a corresponding time course with $T = 1200$. We centered and scaled the subject level time courses for each node before analysis, and verified that each node's time course was stationary using Dickey-Fuller tests. We grouped the brain nodes into one of 6 well known functional brain networks (Akiki and Abdallah, 2019), and fit the VAR model with lag-1 on each of these networks separately. We selected the lag 1 model following previous literature on VAR models applied to fMRI data (Martínez-Montes et al., 2004; Kook et al., 2021), and based on the poor temporal resolution of the fMRI data. We restrict our analysis to a subset of samples with the highest 10% and lowest 10% fluid intelligence scores, with $n = 306$ samples. We note

that the grouping information was only used for post-model fitting comparisons in effective connectivity across groups. We used 1000 burn-in and 4000 MCMC iterations.

To the best of our knowledge, our approach for analyzing fluid intelligence-related effective connectivity differences using heterogeneous multi-subject data is one of the first such attempts. Most existing approaches involve a single-subject VAR analysis, and subsequently these estimates are combined to estimate between-subject variations and examine group differences (Deshpande et al., 2009). There are a handful of approaches for estimating effective connectivity by pooling information across multiple subjects, however they assume known groups (Chiang et al., 2017) with limited heterogeneity within groups, and have similar limitations as outlined in the Introduction. Our analysis using the rgPDPM-VAR model is able to compute effective connectivity for multiple samples without any given group labels and can account for heterogeneity in an unsupervised manner. We compare the performance with a SS-VAR approach that analyses each sample separately, and subsequently performs permutation tests to assess significant differences (10,000 permutations). For both methods, false discovery rate control was applied to obtained significant elements.

In addition to investigating effective connectivity differences, we are interested in the clustering reliability and biological reproducibility of our findings. We report clustering reliability over two distinct MCMC runs, that are designed to evaluate the reliability of the clusters discovered by rgPDPM-VAR. As discussed in the introduction, for high-dimensional multivariate measurements, one can expect a subset of nodes/rows to drive the clustering whereas for other nodes the clustering patterns likely hold little information. We calculate the ARI for the node-level clustering across the two MCMC runs to investigate this aspect of clustering reliability. To assess biological reproducibility, we conduct our VAR analysis for two scans collected from each individual using different phase-encodings (LR1 and RL1), with the expectation that the parameter estimates should be similar correspond-

ing to the two scans. We examine the correlation of the estimated autocovariance elements across the two runs (LR1 and RL1) under both the SS-VAR and the rgPDPM-VAR, with high correlation providing evidence that the findings are reproducible.

5.2 Results

Figure 3 displays heatmaps of the significant autocovariance differences between the low and high FI groups under the rg-PDPMVAR, after appropriate FDR control. Several patterns are clear from Figure 3. First, after FDR control, the rg-PDPMVAR is able to identify a large number of significant differences between the two groups. Second, the rg-PDPMVAR finds a large number of strong differences along the diagonal. These correspond to AR(1) coefficients, and it seems sensible that if there are differences between groups at Lag 1 that they would be strongly related to each nodes' own time course. Thirdly, the strongest differences were observed corresponding to the nodes in the Dorsal Salience network, as illustrated in Table 1. These nodes were identified by looking at columns of the autocovariance matrix with a large proportion of significant elements, which accounts for the varying sizes for the 6 networks. These findings are consistent with previous evidence, which have suggested the dorsal salience and attention networks to be highly related to fluid intelligence (Santarnecchi et al., 2017). We note that in contrast, only one significantly different effective connectivity difference between the high and low fluid intelligence groups was reported under the SS-VAR approach. Such results are clearly biologically implausible since brain connectivity is known to be associated with FI (Finn et al., 2015). Our overall findings point to the advantages of performing a multi-subject analysis accounting for heterogeneity, over a single subject analysis.

To examine biological reproducibility, the right-hand side of Figure 4 displays histograms of the correlations of the rows of the autocovariance matrices across the two analyses corresponding to the LR1 and RL1 fMRI scans, under the SS-VAR and rgPDPM-VAR.

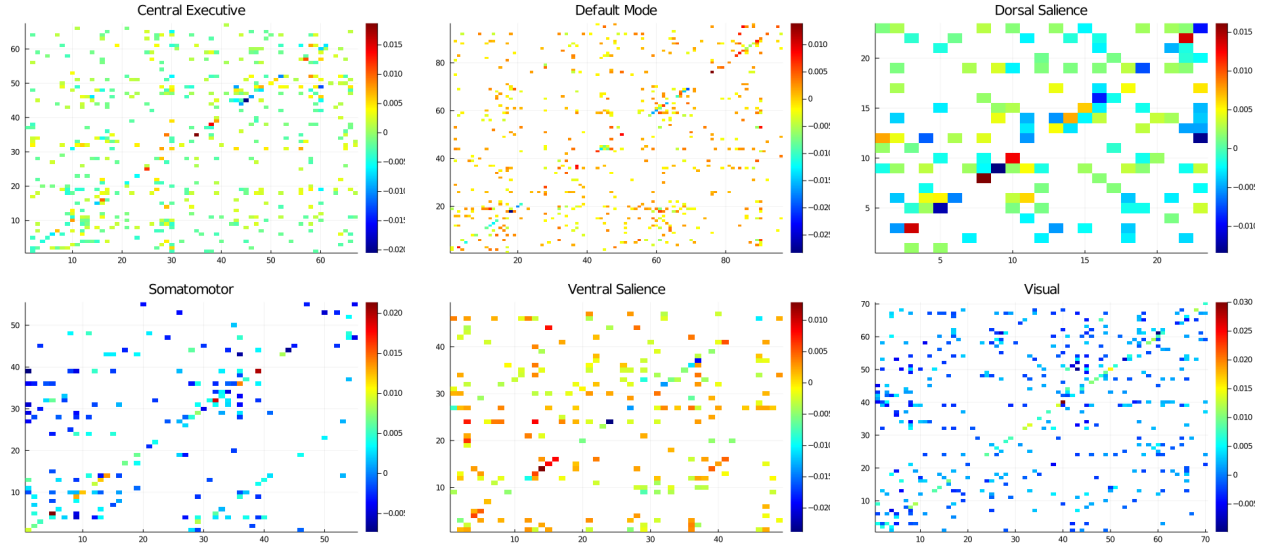


Figure 3: Elements of the autocovariance matrices exhibiting significant differences between the low and high FI groups. The color of the element represents the strength of the mean difference between groups (high FI – low FI), with white elements corresponding to non-significant elements.

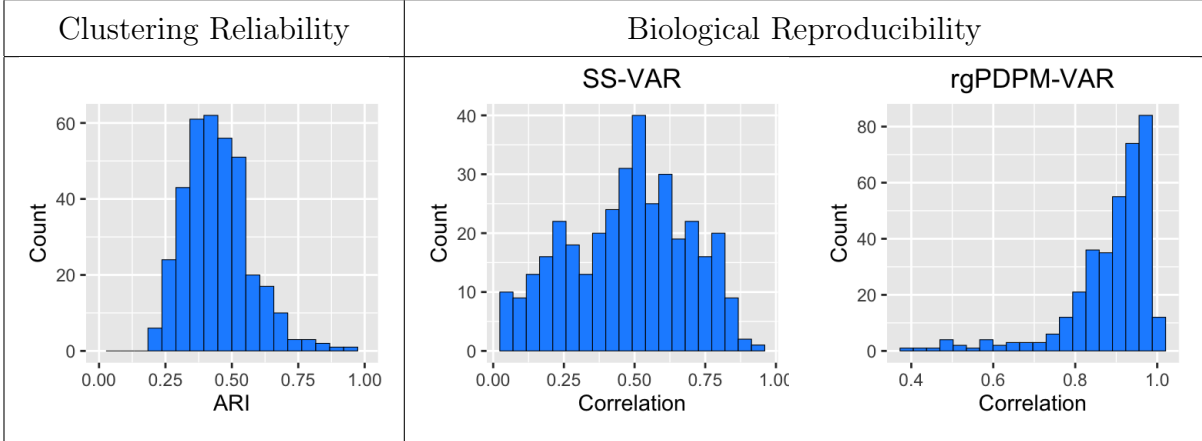


Figure 4: Adjusted Rand index across two runs of the analysis of the HCP LR1 data for assessing clustering reliability (left). Correlation between the rows of A_i across two different HCP data sets (right). The first run of the analysis was on the LR1 phase-encoding data and the second on RL1.

The estimates under the rgPDPM-VAR exhibit a very high degree of correlation, almost entirely > 0.8 . On the other hand, the correlation for the majority of the elements is less than 0.5 under SS-VAR, with only 10 elements registering a correlation greater than 0.8, which implied considerably lower reproducibility overall compared to the multi-subject analysis. Moreover a non-negligible number of nodes had weak reproducibility with correlations less than 0.25 under SS-VAR. In addition, Figure 4 (left) displays a histogram of the ARI for clustering each node across two separate runs of MCMC on the LR1 data, which illustrates clustering reliability. In general, most nodes exhibited 9–10 clusters. As hypothesized in the Introduction, we see a pattern in which a subset of nodes exhibited very high clustering reliability across runs (> 0.7), which supports our hypothesis that only some nodes contribute meaningfully towards clustering of samples. On the other hand, most of the nodes exhibited relatively moderate clustering reliability ($ARI \approx 0.5$), which indicates much higher clustering than chance, but not fully consistent clustering across all subjects corresponding to these nodes. We note that given the strong biological reproducibility results, the moderate or low clustering reliability for a subset of nodes in our analysis should be attributed to the fact that these nodes are irrelevant to clustering. This provides further justification for using the rg-PDPMVAR, which is designed to accommodate exactly this kind of clustering structure. Finally in terms of computation time under the rgPDPM-VAR, a single MCMC iteration on the dorsal salience network required less than 20 seconds of computation time on an 8 core 2021 M1 Macbook Air.

6 Discussion

In this work, we developed a class of novel non-parametric Bayesian VAR models with an ability to flexibly borrow information across heterogeneous samples via unsupervised clustering at multiple scales that bypasses restrictive parametric assumptions and the re-

Node	Network	Prop. FI Diff.	Node	Network	Prop. FI Diff.
L_PF	Dorsal Salience	0.43	R_PFT	Dorsal Salience	0.26
R_7Am	Dorsal Salience	0.35	L_PEF	Dorsal Salience	0.26
L_IFSa	Dorsal Salience	0.35	L_TE2p	Dorsal Salience	0.26
L_PHT	Dorsal Salience	0.35	R_V3A	Visual	0.23
R_PHT	Dorsal Salience	0.30	R_PSL	Ventral Salience	0.22
R_PF	Dorsal Salience	0.30	R_7PL	Dorsal Salience	0.22
L_6a	Dorsal Salience	0.30	R_6r	Dorsal Salience	0.22
L_PFT	Dorsal Salience	0.30	L_7Am	Dorsal Salience	0.22
R_PGs	Central Executive	0.28	L_6r	Dorsal Salience	0.22
R_IFSa	Dorsal Salience	0.26	L_V3A	Visual	0.21

Table 1: Table of the 20 nodes with large proportion of significant effects on other nodes within their network. Note that the proportion is used instead of the raw count to account for the different network sizes.

quirement of replicated samples, and provide distinct advantages over existing multi-subject VAR approaches. We illustrated posterior consistency properties for the proposed PDPM-VAR approach and variants via novel theoretical results for matrix variate data, and implemented the approaches via an efficient MCMC sampling scheme. Through extensive simulations, we showed a superior numerical performance under the proposed methods compared to a single subject analysis, even when the latter is augmented via an additional adhoc clustering step that is designed to borrow information across similar samples. In addition, the rgPDPM-VAR variant often had superior performance compared to the other PDPM variants in heterogeneous data settings, and it produced biologically interpretable and reproducible parameter estimates in our analysis of the HCP data compared to single subject analysis. Overall, we found that the proposed rgPDPM-VAR, which clusters rows of the subject-level autocovariance matrices, was able to perform well in nearly all settings.

While this work introduced several variants of the PDPM-VAR model, there are numerous potential extensions that lie within our class of models. In particular, future directions

might investigate possible generalizations intended to induce sparsity in the parameter estimates. For example, a spike and slab prior could be used to model the autocovariance elements, with the slab component modeled using a DP mixtures. Additionally, the models could be generalized to accommodate even higher levels of heterogeneity, such as clustering individual autocovariance elements separately. However, such extensions may involve a massive computational burden. The proposed approaches, particularly the rgPDPM-VAR, seems to strike a desirable balance between computational complexity, clustering flexibility and model parsimony, with theoretical guarantees and appealing practical performance. Finally, we note that the proposed product of DP priors provides a viable improvement over traditional DP mixture models and it should have wide applicability to other types of settings that go beyond the VAR framework, which is of immediate interest in this article. We expect to pursue these directions in future research.

SUPPLEMENTARY MATERIAL

Supplementary Materials: PDF file containing additional proofs, lemmas, computation details, and simulation results.

References

Agrawal, R., Gehrke, J., Gunopulos, D., and Raghavan, P. (2005). Automatic subspace clustering of high dimensional data. *Data Mining and Knowledge Discovery*, 11(1):5–33.

Akiki, T. J. and Abdallah, C. G. (2019). Determining the hierarchical architecture of the human brain using subject-level clustering of functional networks. *Scientific reports*, 9(1):1–15.

Billio, M., Casarin, R., and Rossini, L. (2019). Bayesian nonparametric sparse VAR models. *Journal of Econometrics*, 212(1):97–115.

Bradley, J. R., Holan, S. H., and Wikle, C. K. (2015). Multivariate spatio-temporal models for high-dimensional areal data with application to longitudinal employer-household dynamics. *The Annals of Applied Statistics*, 9(4):1761–1791.

Canale, A. and De Blasi, P. (2017). Posterior asymptotics of nonparametric location-scale mixtures for multivariate density estimation. *Bernoulli*, 23(1):379–404.

Chiang, S., Guindani, M., Yeh, H. J., Haneef, Z., Stern, J. M., and Vannucci, M. (2017). Bayesian vector autoregressive model for multi-subject effective connectivity inference using multi-modal neuroimaging data. *Human Brain Mapping*, 38(3):1311–1332.

Cramer, R. H. and Miller, R. B. (1978). Multivariate time series analysis of bank financial behavior. *Journal of Financial and Quantitative Analysis*, 13(5):1003–1017.

Dahl, C. M. and González-Rivera, G. (2003). Testing for neglected nonlinearity in regression models based on the theory of random fields. *Journal of Econometrics*, 114(1):141–164.

Deshpande, G., LaConte, S., James, G. A., Peltier, S., and Hu, X. (2009). Multivariate Granger causality analysis of fMRI data. *Human brain mapping*, 30(4):1361–1373.

Doan, T., Litterman, R., and Sims, C. (1984). Forecasting and conditional projection using realistic prior distributions. *Econometric reviews*, 3(1):1–100.

Durante, D., Dunson, D., and Vogelstein, J. (2017). Nonparametric Bayes modeling of populations of networks. *Journal of the American Statistical Association*, 112(520):1516–1530.

Edelman, A. (1988). Eigenvalues and condition numbers of random matrices. *SIAM journal on matrix analysis and applications*, 9(4):543–560.

Engle, R. and Watson, M. (1981). A one-factor multivariate time series model of metropolitan wage rates. *Journal of the American Statistical Association*, 76(376):774–781.

Finn, E. S., Shen, X., Scheinost, D., Rosenberg, M. D., Huang, J., Chun, M. M., Papademetris, X., and Constable, R. T. (2015). Functional connectome fingerprinting: identifying individuals using patterns of brain connectivity. *Nature neuroscience*, 18(11):1664–1671.

Gefang, D. (2014). Bayesian doubly adaptive elastic-net lasso for VAR shrinkage. *International Journal of Forecasting*, 30(1):1–11.

Ghosal, S. and Van Der Vaart, A. (2007). Posterior convergence rates of Dirichlet mixtures at smooth densities. *The Annals of Statistics*, 35(2):697–723.

Ghosh, J. and Dunson, D. B. (2009). Default prior distributions and efficient posterior computation in Bayesian factor analysis. *Journal of Computational and Graphical Statistics*, 18(2):306–320.

Ghosh, S., Khare, K., and Michailidis, G. (2018). High-dimensional posterior consistency in Bayesian vector autoregressive models. *Journal of the American Statistical Association*, 114(526):735–748.

Gorrostieta, C., Fiecas, M., Ombao, H., Burke, E., and Cramer, S. (2013). Hierarchical vector auto-regressive models and their applications to multi-subject effective connectivity. *Frontiers in computational neuroscience*, 7:159.

Han, F., Lu, H., and Liu, H. (2015). A direct estimation of high dimensional stationary vector autoregressions. *Journal of Machine Learning Research*, 16(97):3115–3150.

Hinton, G. E. (2002). Training products of experts by minimizing contrastive divergence. *Neural computation*, 14(8):1771–1800.

Jeliazkov, I. (2013). Nonparametric vector autoregressions: Specification, estimation, and inference. In *VAR Models in Macroeconomics–New Developments and Applications: Essays in Honor of Christopher A. Sims*. Emerald Group Publishing Limited.

Kalli, M. and Griffin, J. E. (2018). Bayesian nonparametric vector autoregressive models. *Journal of Econometrics*, 203(2):267–282.

Kook, J. H., Vaughn, K. A., DeMaster, D. M., Ewing-Cobbs, L., and Vannucci, M. (2021). Bvar-connect: A variational Bayes approach to multi-subject vector autoregressive models for inference on brain connectivity networks. *Neuroinformatics*, 19:39–56.

Korobilis, D. (2013). Var forecasting using Bayesian variable selection. *Journal of Applied Econometrics*, 28(2):204–230.

Kundu, S. and Risk, B. B. (2021). Scalable Bayesian matrix normal graphical models for brain functional networks. *Biometrics*, 77(2):439–450.

Lanne, M. and Lütkepohl, H. (2010). Structural vector autoregressions with nonnormal residuals. *Journal of Business & Economic Statistics*, 28(1):159–168.

Lu, F., Zheng, Y., Cleveland, H., Burton, C., and Madigan, D. (2018). Bayesian hierarchical vector autoregressive models for patient-level predictive modeling. *PLoS one*, 13(12):e0208082.

Lütkepohl, H. (2005). *New introduction to multiple time series analysis*. Springer Science & Business Media.

Martínez-Montes, E., Valdés-Sosa, P., Miwakeichi, F., Goldman, R., and Cohen, M. (2004). Concurrent eeg/fmri analysis by multiway partial least squares. *Neuroimage*, 22:1023–1034.

Park, T. and Casella, G. (2008). The Bayesian lasso. *Journal of the American Statistical Association*, 103(482):681–686.

Rand, W. M. (1971). Objective criteria for the evaluation of clustering methods. *Journal of the American Statistical Association*, 66(336):846–850.

Rousseeuw, P. J. (1987). Silhouettes: a graphical aid to the interpretation and validation of cluster analysis. *Journal of computational and applied mathematics*, 20:53–65.

Santarnecchi, E., Emmendorfer, A., Tadayon, S., Rossi, S., Rossi, A., and Pascual-Leone, A. (2017). Network connectivity correlates of variability in fluid intelligence performance. *Intelligence*, 65:35–47.

Schwartz, L. (1965). On Bayes procedures. *Zeitschrift für Wahrscheinlichkeitstheorie und verwandte Gebiete*, 4(1):10–26.

Sethuraman, J. (1994). A constructive definition of Dirichlet priors. *Statistica Sinica*, pages 639–650.

Shen, W., Tokdar, S. T., and Ghosal, S. (2013). Adaptive Bayesian multivariate density estimation with Dirichlet mixtures. *Biometrika*, 100(3):623–640.

Smith, S. M., Beckmann, C. F., Andersson, J., Auerbach, E. J., Bijsterbosch, J., Douaud, G., Duff, E., Feinberg, D. A., Griffanti, L., Harms, M. P., et al. (2013). Resting-state fmri in the human connectome project. *Neuroimage*, 80:144–168.

Tokdar, S. T. (2006). Posterior consistency of Dirichlet location-scale mixture of normals in density estimation and regression. *Sankhyā: The Indian Journal of Statistics*, 69(1):90–110.

Walker, S. G. (2007). Sampling the Dirichlet mixture model with slices. *Communications in Statistics—Simulation and Computation*, 36(1):45–54.

Weise, C. L. (1999). The asymmetric effects of monetary policy: A nonlinear vector autoregression approach. *Journal of Money, Credit and Banking*, 31(1):85–108.

Wu, Y. and Ghosal, S. (2008). Kullback Leibler property of kernel mixture priors in Bayesian density estimation. *Electronic Journal of Statistics*, 2:298–331.

Supplementary Materials

7 Posterior Computation Steps

7.1 Residual Covariance Updates:

Following Ghosh and Dunson (2009), we use a parameter expanded approach to facilitate sampling parameters $(\boldsymbol{\Gamma}_i, \boldsymbol{\Psi}_i)$ corresponding to Σ_i . Denoting $\boldsymbol{\Xi}_i = \text{diag}\{\xi_{i,1}, \dots, \xi_{i,B}\}$, we use the following working model:

$$\mathbf{x}_{i,t} = \sum_{k=1}^{\min\{t-1, K\}} A_{ik} \mathbf{x}_{i,t-k} + \boldsymbol{\Gamma}_i^* \boldsymbol{\eta}_{i,t}^* + \boldsymbol{\epsilon}_{i,t}^*, \quad \boldsymbol{\eta}_{i,t}^* \sim N(0, \boldsymbol{\Xi}_i), \quad \boldsymbol{\epsilon}_{i,t}^* \sim N(0, \boldsymbol{\Psi}_i),$$

where $\boldsymbol{\Gamma}_i^*$ is a lower triangular matrix without constraints. The residual covariance $\Sigma_i = \boldsymbol{\Gamma}_i \boldsymbol{\Gamma}_i' + \boldsymbol{\Psi}_i$ can be directly recovered from this working model as described in Ghosh and Dunson (2009) by transforming: $\boldsymbol{\Gamma}_{i,d',b} = \text{sign}(\boldsymbol{\Gamma}_{i,b,b}^*) \boldsymbol{\Gamma}_{i,d',b}^* \xi_{i,b}^{1/2}$ and $\eta_{i,t,b} = \text{sign}(\boldsymbol{\Gamma}_{i,b,b}^*) \xi_{i,b}^{-1/2} \eta_{i,t,b}$, where $\boldsymbol{\Gamma}_{i,d',b}$ is the d' th row, b th element of $\boldsymbol{\Gamma}_i$ and $\eta_{i,t,b}$ is the b th element of $\boldsymbol{\eta}_{i,t}$.

Under the low rank representation, we impose DP mixture priors on $(\boldsymbol{\Gamma}_i^*, \boldsymbol{\Xi}_i, \boldsymbol{\Psi}_i)$ leading to a mixture prior on Σ_i . This corresponds to the prior $\Sigma_i \sim \sum_{h_\sigma=1}^{\infty} \pi_{\sigma, h_\sigma} \delta_{(\boldsymbol{\Gamma}_{h_\sigma}^*, \boldsymbol{\Xi}_{h_\sigma}, \boldsymbol{\Psi}_{h_\sigma})}$, where $(\boldsymbol{\Gamma}_{h_\sigma}^*, \boldsymbol{\Xi}_{h_\sigma}, \boldsymbol{\Psi}_{h_\sigma}) \sim P_2^* \equiv P_{\boldsymbol{\Gamma}^*} \times P_{\boldsymbol{\Xi}} \times P_{\boldsymbol{\Psi}}$. Here $P_{\boldsymbol{\Gamma}^*}$ is a product of independent standard normal distributions, $P_{\boldsymbol{\Xi}}$ is a product of independent $\text{Gamma}(1/2, 1/2)$ distributions yielding a half-Cauchy prior on the diagonal elements of $\boldsymbol{\Gamma}$ and a Cauchy prior on the lower-off-diagonal elements of $\boldsymbol{\Psi}$ as in Ghosh and Dunson (2009), and the inverse of the diagonal elements of $\boldsymbol{\Psi}$ have independent $\text{Gamma}(\alpha_\sigma, \beta_\sigma)$ priors. Note that here $\boldsymbol{\Gamma}_i^*$ is not a square matrix, and by diagonal elements we refer to elements $\Gamma_{i,1,1}, \dots, \Gamma_{i,B,B}$.

Under the stick-breaking representation of Sethuraman (1994), we can write $\pi_{\sigma, h_\sigma} = \nu_{\sigma, h_\sigma} \prod_{l_\sigma=1}^{h_\sigma-1} (1 - \nu_{\sigma, l_\sigma})$, $\nu_{l_\sigma} \sim \text{Beta}(1, \alpha_2)$. We use the slice sampling approach of Walker (2007) to facilitate sampling. This approach introduces a cluster membership indicator, V , with $V_i = h_\sigma$ when subject i belongs to cluster h_σ , and let $\mathcal{V}_{h_\sigma} = \{i : V_i = h_\sigma\}$ be the

indices of all subjects belonging to covariance cluster h_σ and let n_{σ,h_σ} be the cardinality of this set. Let g_i be a uniformly distributed latent variable used to reduce the stick-breaking representation of the DPM to a finite sum. Our sampler updates ν_{σ,h_σ} , and g_i as:

$$\nu_{\sigma,h_\sigma} | \{V_1, \dots, V_N\} \sim \text{Beta} \left(1 + n_{\sigma,h_\sigma}, \alpha_2 + \sum_{i=1}^N I_{(V_i > \nu_{\sigma,h_\sigma})} \right), \quad g_i | V_i \sim U(0, \pi_{\sigma,V_i}).$$

The cluster membership indicators V_i are then sampled from a multinomial distribution with posterior probabilities $(p(V_i = 1 | -), \dots, p(V_i = h_\sigma^* | -))$ expressed as,

$$p(V_i = h_\sigma^* | -) \sim \frac{I_{(g_i < \pi_{\sigma,h_\sigma})} \prod_{t=1}^{T_i} \phi_{\Sigma_{h_\sigma}}(x_{i,t}; A_{i1}, \dots, A_{iK})}{\sum_{h'_\sigma=1}^{h_\sigma^*} \left\{ I_{(g_i < \pi_{\sigma,h'_\sigma})} \prod_{t=1}^{T_i} \phi_{\Sigma_{h'_\sigma}}(x_{i,t}; A_{i1}, \dots, A_{iK}) \right\}},$$

where $h_\sigma^* = \min\{h_\sigma : g_i > 1 - \sum_{h'_\sigma=1}^{h_\sigma} \pi_{\sigma,h'_\sigma}\}$, for all i . Conditioned on the cluster memberships, it is straightforward to update the variables in the low rank representation of Σ using an extension of the approach outlined in Ghosh and Dunson (2009). We start by sampling the elements of $\Gamma_{h_\sigma^*}$ one row at a time from their full conditionals:

$$\begin{aligned} \Gamma_{h_\sigma,d'}^* | - &\sim N \left(\mu_{\Gamma_{h_\sigma,d'}^*}, \Sigma_{\Gamma_{h_\sigma,d'}^*} \right), \text{ where } \Sigma_{\Gamma_{h_\sigma,d'}^*} = \left(\sigma_{h_\sigma,d'}^{-2} \sum_{i \in \mathcal{V}_{h_\sigma}} \sum_{t=1}^{T_i} (\mathcal{E}_{\eta,itd'}^*)' (\mathcal{E}_{\eta,itd'}^*) + I_{\min\{d', B\}} \right)^{-1}, \\ \mu_{\Gamma_{h_\sigma,d'}^*} &= \Sigma_{\Gamma_{h_\sigma,d'}^*} \left(\sigma_{h_\sigma,d'}^{-2} \sum_{i \in \mathcal{V}_{h_\sigma}} \sum_{t=1}^{T_i} \mathcal{E}_{\eta,itd'}^* \left[x_{i,t}^{(d')} - A_{i,d'} \bullet \mathbf{z}_{i,t} \right] \right), \quad \mathcal{E}_{\eta,itd'}^* = (\eta_{i,t,1}^*, \dots, \eta_{i,t,\min\{d', B\}}^*)', \end{aligned}$$

$x_{i,t}^{(d)}$ is the response for the i th subject at the d 'th node and t th time point, and $A'_{ik,d'} \bullet$ is the transpose of the d 'th row of A_{ik} , $A_{i,d'} \bullet$ is the $DK \times 1$ vector formed by stacking the $A'_{ik,d'} \bullet$ across all lags, and $\mathbf{z}_{i,t} = [\mathbf{x}'_{i,t-1}, \dots, \mathbf{x}'_{i,t-K}]'$ is the $DK \times 1$ vector of previous outcomes used to predict the outcome at time t , padded with zeros for the case that $t - k < 1$.

The full conditionals for the remaining terms in the lower rank representation for Σ_i

are given by:

$$\eta_{i,t}^* | \sim N \left(\mu \eta_{i,t}^*, \Sigma \eta_{i,t}^* \right), \quad \xi_{h_\sigma, b} | \sim Gamma \left(\frac{1 + N_{h_\sigma}}{2}, \frac{1}{2} \left[1 + \sum_{i \in \mathcal{V}_{h_\sigma}} \sum_{t=1}^{T_i} \eta_{i,t,b}^{*2} \right] \right),$$

$$\sigma_{h_\sigma, d'}^{-2} | \sim Gamma \left(a_\sigma + \frac{N_{h_\sigma}}{2}, b_\sigma + \frac{1}{2} \sum_{i \in \mathcal{V}_{h_\sigma}} \sum_{t=1}^{T_i} \left[x_{i,t}^{(d')} - A_{i,d',\bullet} \mathbf{z}_{i,t} - \boldsymbol{\Gamma}_{i,d'}^* \boldsymbol{\eta}_{i,t}^* \right]^2 \right)$$

where N_{h_σ} is equal to the total number of time points across all subjects in covariance cluster h_σ , and $\Sigma \eta_{i,t}^* = (\boldsymbol{\Xi}_{V_i}^{-1} + \boldsymbol{\Gamma}_{V_i}' \boldsymbol{\Psi}_{V_i} \boldsymbol{\Gamma}_{V_i})^{-1}$ and $\mu \eta_{i,t}^* = \Sigma \eta_{i,t}^* \boldsymbol{\Gamma}_{V_i}' \boldsymbol{\Psi}_{V_i} \left[x_{i,t}^{(d')} - A_{i,d',\bullet} \mathbf{z}_{i,t} \right]$.

7.2 Autocovariance Parameter Updates

We outline the posterior computation steps for the autocovariance parameters using the base measure that corresponds to independent double exponential prior with shrinkage parameter λ on the elements of the autocovariance matrices.

7.2.1 Computation Steps for PDPM-VAR

As with the covariance terms, we use the stick-breaking representation (Sethuraman, 1994) of the Dirichlet process to enable posterior computation under the DPM priors. For the autocovariance terms, we can express the prior as,

$$A_i | P_\Theta \sim P_\Theta, \quad P_\Theta = \sum_{h_1=1}^{\infty} \pi_{h_1} \delta_{A_h}$$

where $\pi_{h_1} = \nu_{h_1} \prod_{l_1 < \nu_{h_1}} (1 - \nu_{l_1})$, $\nu_{h_1} \sim Beta(1, \alpha_1)$, and $A_h \sim P_1^*$, where P_1^* is a multivariate normal distribution with mean $\mathbf{0}$ and variance $\text{diag}\{\boldsymbol{\tau}^2\}$. The prior for the individual τ^2 terms is given by $p(\tau_{k,d'}^2) = \frac{\lambda^2}{2} \exp\{-\frac{1}{2}\lambda^2\tau_{k,d'}^2\}$, which implies a double exponential base measure for modeling the autocovariance terms (Park and Casella, 2008). Furthermore, we place a conjugate $Gamma(r, \delta)$ hyperprior on λ^2 to facilitate Gibbs sampling. Throughout our applications we fix $r = 1.0$ and $\delta = 2.0$, which yield good performance in a wide range of settings. As with the residual covariance, we use the slice sampling approach of Walker

(2007) to facilitate sampling from this infinite mixture. Let H_1 be a cluster membership indicator, where $H_{1,i} = h_1$ if subject i belongs to the h_1 th autocovariance matrix cluster. Let $\mathcal{H}_{h_1} = \{i : H_{1,i} = h_1\}$ be the indices of all subjects belonging to autocovariance cluster h_1 , with n_{h_1} being the cardinality of this set. The sampler proceeds by introducing a latent uniform variable u_i , relating the cluster memberships to the stick breaking representation of the DPM. The sampler proceeds by iteratively sampling ν_{h_1} and $u_{1,i}$ from their full conditionals,

$$\nu_{h_1} | \{H_{1,i}\} \sim Beta \left(1 + n_{h_1}, \alpha_1 + \sum_{i=1}^N I_{(H_{1,i} > h_1)} \right), \quad u_{1,i} | \nu_{h_1}, H_{1,i} \sim U(0, \pi_{H_{1,i}}).$$

The cluster memberships, $H_{1,i}$, are then sampled from a multinomial distribution with posterior probabilities $(P(H_{1,i} = 1 | -), \dots, P(H_{1,i} = h_1^* | -))$ given by:

$$P(H_{1,i} = h_1 | -) = \frac{I_{(u_{1,i} < \pi_{h_1})} \prod_{t=1}^{T_i} \phi_{\Sigma_{V_i}} \left(\mathbf{x}_{i,t} - \sum_{k=1}^K A_{k,h_1} \mathbf{x}_{i,t-k} \right)}{\sum_{h_1'=1}^{h_1^*} \left\{ I_{(u_{1,i} < \pi_{h_1'})} \prod_{t=1}^{T_i} \phi_{\Sigma_{V_i}} \left(\mathbf{x}_{i,t} - \sum_{k=1}^K A_{k,h_1'} \mathbf{x}_{i,t-k} \right) \right\}}$$

where $h_1^* = \min\{h_1 : u_{1,i} > 1 - \sum_{h_1'=1}^{h_1} \pi_{A,h_1'}, \text{ for all } i\}$.

Conditioned on the cluster memberships, we sample the autocovariance matrices across all lags one outcome at a time. The full conditional for $A_{h_1,d' \bullet}$ is given by $A_{h_1,d' \bullet} | - \sim N(\boldsymbol{\mu}_{A_{h_1},d'}^*, \boldsymbol{\Sigma}_{A_{h_1},d'}^*)$ with variance and mean: $\boldsymbol{\Sigma}_{A_{h_1},d'}^* = \left(\sum_{i \in \mathcal{H}_{h_1}} \sum_{t=1}^{T_i} \sigma_{i,d'}^{-2} \mathbf{z}_{i,t} \mathbf{z}_{i,t}' + \boldsymbol{\Lambda}_D^{-1} \right)^{-1}$, $\boldsymbol{\mu}_{A_{h_1},d'}^* = \boldsymbol{\Sigma}_{A_{h_1},d'}^* \left\{ \sum_{i \in \mathcal{H}_{h_1}} \sum_{t=1}^{T_i} \left[\sigma_{i,d'}^{-2} \mathbf{z}_{i,t} \left(x_{i,t}^{(d')} - \boldsymbol{\Gamma}_{i,d'}^* \boldsymbol{\eta}_{i,t}^* \right) \right] \right\}$, respectively.

Finally, the parameters of the double exponential base measure can be updated using the approach outlined in Park and Casella (2008). The variance term in the base measure can be sampled from an inverse Gaussian distribution, $\tau_{k,d'}^{-2} \sim InverseGaussian \left(\sqrt{\frac{\lambda^2}{C \bar{A}_{k,d'}^2}}, \lambda^2 \right)$, for $k = 1, \dots, K$ and $d' = 1, \dots, D^2$, where C is the number of clusters. The posterior distribution for the lasso parameter is a gamma distribution, $\lambda^2 | \boldsymbol{\tau}^2 \sim Gamma(KD^2 + r, \delta + \sum_{k=1}^K \sum_{d'=1}^{D^2} \frac{\tau_{k,d'}^2}{2})$.

7.2.2 Computation Steps for rgPDPM-VAR

The rgDPM-VAR requires some modification to the slice sampling approach. In particular, the sampler for the rgDPM-VAR extends the latent terms in the slice sampler along the outcome dimension. Let $H_{1d'}$ be the vector of autocovariance cluster indices for outcome d' , with $H_{1d',i} = h_{1,d'}$ when subject i belongs to outcome d' cluster $h_{1,d'}$, and let $\mathcal{H}_{h_{1,d'}} = \{i : H_{1d',i} = h_{1,d'}\}$ be the indices of all subjects belonging to outcome d' cluster $h_{1,d'}$, with $n_{h_{1,d'}}$ being the cardinality of this set. Then we have the following full conditionals:

$$\nu_{h_{1,d'}} | \{H_{1d',i}\} \sim \text{Beta} \left(1 + n_{d',h}, \alpha_1 + \sum_{i=1}^N I_{(H_{1d',i} > h_{1,d'})} \right), \quad u_{1d',i} | \nu_{h_{1,d'}}, H_{1d',i} \sim U(0, \pi_{d',H_{1d',i}})$$

The cluster memberships, $H_{1d',i}$, are then sampled from a multinomial distribution with posterior probabilities $(P(H_{1d',i} = 1 | -), \dots, P(H_{1d',i} = h_{1,d'}^* | -))$ given by:

$$P(H_{1d',i} = h_{1,d'} | -) = \frac{I_{(u_{1d',i} < \pi_{d',h_{1,d'}})} \prod_{t=1}^{T_i} \phi_{\Sigma_{V_i}} \left(x_{i,t}^{(d')} - \sum_{k=1}^K A_{k,h_{1d'}} \mathbf{x}_{t-k} \right)}{\sum_{h_{1,d'}^*=1}^{h_{1,d'}} \left\{ I_{(u_{1d',i} < \pi_{d',h_{1,d'}})} \prod_{t=1}^{T_i} \phi_{\Sigma_{V_i}} \left(x_{i,t}^{(d')} - \sum_{k=1}^K A_{k,h_{1,d'}} \mathbf{x}_{t-k} \right) \right\}},$$

where $h_{1,d'}^* = \min\{h : u_{1d',i} > 1 - \sum_{h_{1,d'}=1}^h \pi_{d',h_{1,d'}}, \text{ for all } i\}$. Conditioned on the cluster memberships, the autocovariance terms can be updated in an identical manner to the PDPM-VAR. When updating the parameters of the double exponential base measure the variance terms can be sampled from inverse Gaussian distributions: $\tau_{k,d',d^*}^{-2} \sim \text{InverseGaussian} \left(\sqrt{\frac{\lambda_{d'}^2}{C_{d'} A_{k,d',d^*}^2}}, \lambda_{d'}^2 \right)$ for $k = 1, \dots, K$, $d^* = 1, \dots, D$ and $d' = 1, \dots, D$, where $C_{d'}$ is the number of autocovariance clusters for outcome d' and τ_{k,d',d^*}^{-2} is the variance term corresponding to the d^* th element of the d' th row of A_k , and \bar{A}_{k,d',d^*} is the average of element d^* of the d' th row of A_k across the $C_{d'}$ clusters. The outcome-specific lasso parameters have gamma posteriors: $\lambda_{d'}^2 | \boldsymbol{\tau}_{k,d',d^*}^2 \sim \text{Ga}(DK + r, \delta + \sum_{k=1}^K \sum_{d^*=1}^D \frac{\tau_{k,d',d^*}^2}{2})$ for $d' = 1, \dots, D$.

7.2.3 Computation Steps for lgPDPM-VAR

The sampling steps under the lgPDPM-VAR model proceeds in a similar manner as the other variants outlined in the manuscript. The main difference with other variants is clustering now takes place over lags instead of the entire autocorrelation matrix. To accommodate this, we introduce lag-specific subscripts into our slice sampler terms. Let H_{1k} be the vector of autocorrelation cluster indices for lag k , with $H_{1k,i} = h_{1,k}$ when subject i belongs to cluster $h_{1,k}$, and let $\mathcal{H}_{h_{1,k}} = \{i : H_{1k,i} = h_{1,k}\}$ be the indices of all subjects belonging to lag k cluster $h_{1,k}$, with $n_{h_{1,k}}$ being the cardinality of this set. The sampler proceeds by sampling $\nu_{h_{1,k}}$ and $u_{1k,i}$ from their full conditionals:

$$\nu_{h_{1,k}} | \{H_{1k,i}\} \sim \text{Beta} \left(1 + n_{h_{1,k}}, \alpha_1 + \sum_{i=1}^N I_{(H_{1k,i} > h_{1,k})} \right), \quad u_{1k,i} | \nu_{h_{1,k}}, H_{1k,i} \sim U(0, \pi_{k, H_{1k,i}})$$

The cluster memberships, $H_{1k,i}$, are then sampled from a multinomial distribution with posterior probabilities $(P(H_{1k,i} = 1 | -), \dots, P(H_{1k,i} = h_{1,k}^* | -))$ given by:

$$P(H_{1k,i} = h_{1,k}) | - = \frac{I_{(u_{1k,i} < \pi_{k, h_{1,k}})} \prod_{t=1}^{T_i} \phi_{\Sigma_{V_i}} \left(\mathbf{x}_{i,t} - \sum_{\ell \neq k} A_{\ell, h_{1,k}} \mathbf{x}_{i,t-\ell} - A_{k, h_{1,k}} \mathbf{x}_{i,t-k} \right)}{\sum_{h_{1,k}^*=1}^h \left\{ I_{(u_{1k,i} < \pi_{k, h_{1,k}^*})} \prod_{t=1}^{T_i} \phi_{\Sigma_{V_i}} \left(\mathbf{x}_{i,t} - \sum_{\ell \neq k} A_{\ell, h_{1,k}^*} \mathbf{x}_{i,t-\ell} - A_{k, h_{1,k}^*} \mathbf{x}_{i,t-k} \right) \right\}}$$

where $h_{1,k}^* = \min\{h : u_{1k,i} > 1 - \sum_{h_{1,k}^*=1}^h \pi_{k, h_{1,k}^*}, \text{ for all } i\}$. To sample the autoregression terms corresponding to a single outcome, we sample across all lags and clusters simultaneously. We do this by redefining our z and A terms as follows. Let C_1, \dots, C_K be the number of autoregressive coefficient clusters for lags $1, \dots, K$, respectively. Define $\mathbf{z}_{i,t}^*$ to be a vector of length $D \sum_{k=1}^K C_k$ vector, and let $\mathcal{C} = \{c_{1,1}, \dots, c_{1,C_1}, c_{2,1}, \dots, c_{K,C_K}\}$ be a partition of the indices of $\mathbf{z}_{i,t}^*$ s.t. $c_{k,h} = \{\sum_{k'=1}^{h-1} C_{k'} D + (h-1)D + 1, \dots, \sum_{k'=1}^{h-1} C_{k'} D + hD\}$. Then, set elements $c_{k, H_{1k,i}}$ of $\mathbf{z}_{i,t}^* = \mathbf{z}_{i,t}$ for each k and let all other elements be 0. Similarly, let $A_{d', \bullet}^*$ be a vector of length $D \sum_{k=1}^K C_k$ vector with elements $c_{k,h}$ of $A_{d', \bullet}^* = A'_{k, h_{1,k}, d'}$. Then, the mean for $x_{i,t}^{(d')} = A_{d', \bullet}^{*'} \mathbf{z}_{i,t}^*$, and we can sample the entire $A_{d', \bullet}^*$ at once as,

$$A_{d',\bullet}^* | - \sim N(\boldsymbol{\mu}_{A,d'}^*, \boldsymbol{\Sigma}_{A,d'}^*), \text{ with variance and mean: } \boldsymbol{\Sigma}_{A,d'}^* = \left(\sum_{t=1}^{T_i} \sigma_{i,d'}^{-2} \mathbf{z}_{i,t}^* \mathbf{z}_{i,t}^{*'} + \mathbf{D}_D \right)^{-1},$$

$$\boldsymbol{\mu}_{A,d'}^* = \boldsymbol{\Sigma}_{A,d'}^* \left\{ \sum_{t=1}^{T_i} \sigma_{i,d'}^{-2} \mathbf{z}_{i,t}^* \left(x_{i,t}^{(d')} - \boldsymbol{\Gamma}_{i,d'}^* \boldsymbol{\eta}_{i,t}^* \right) \right\}.$$

When updating the parameters of the double exponential base measure the variance term can be sampled from an inverse Gaussian distribution: $\tau_{k,d'}^{-2} \sim \text{InverseGaussian} \left(\sqrt{\frac{\lambda_k^2}{C_k A_{k,d'}^2}}, \lambda_k^2 \right)$ for $k = 1, \dots, K$ and $d' = 1, \dots, D^2$. The posterior distribution for the shrinkage parameter is again a gamma distribution: $\lambda_k^2 | \boldsymbol{\tau}_k^2 \sim \text{Gamma}(D^2 + r, \delta + \sum_{d'=1}^{D^2} \frac{\tau_{k,d'}^2}{2})$ for $k = 1, \dots, K$.

8 Additional Simulation Results

Simulation results for the $D = 40, T = 250$ case with 75% sparsity are presented in Figures 5–6. Results for the $D = 40, T = 250$ case with 90% sparsity are presented in Figures 7–8. Results for the $D = 40, T = 250, 350$ case with 75% sparsity are presented in Figures 9–10. Results for the $D = 40, T = 250, 350$ case with 90% sparsity are presented in Figures 11–12. Simulation results for the $D = 100, T = 250$ case with 75% sparsity are presented in the main manuscript. Results for the $D = 100, T = 250$ case with 90% sparsity are presented in Figures 13–14. Results for the $D = 100, T = 250, 350$ case with 75% sparsity are presented in Figures 15–16. Results for the $D = 100, T = 250, 350$ case with 90% sparsity are presented in Figures 17–18.

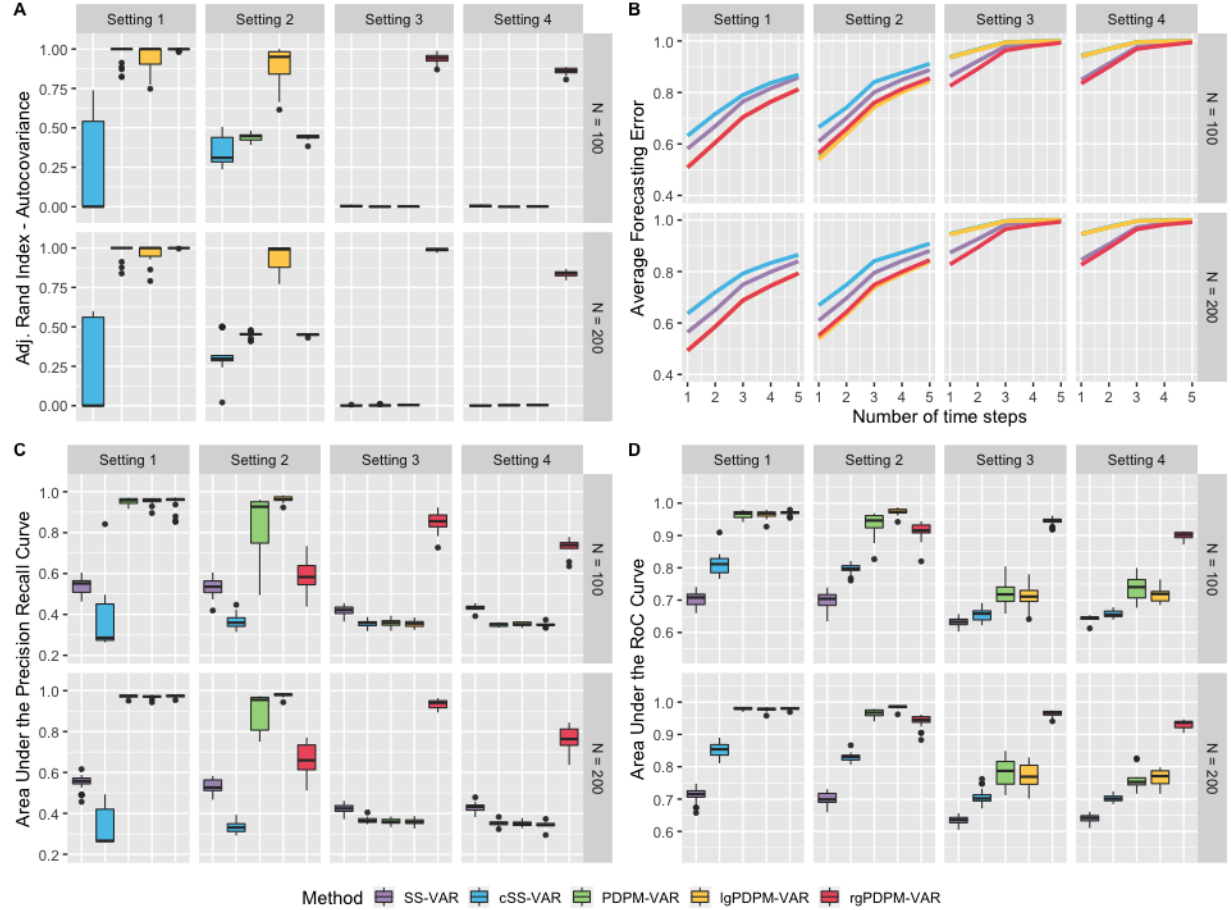


Figure 5: Simulation results for the $D = 40$, $T = 250$ case with sparsity level 0.75. Panel A displays the adjusted Rand index for clustering the autocovariance matrices. Panel B displays the forecasting error at 1–5 time steps. Panels C and D display the area under the PR and RoC curves for identifying non-zero elements of the autocovariance matrices.

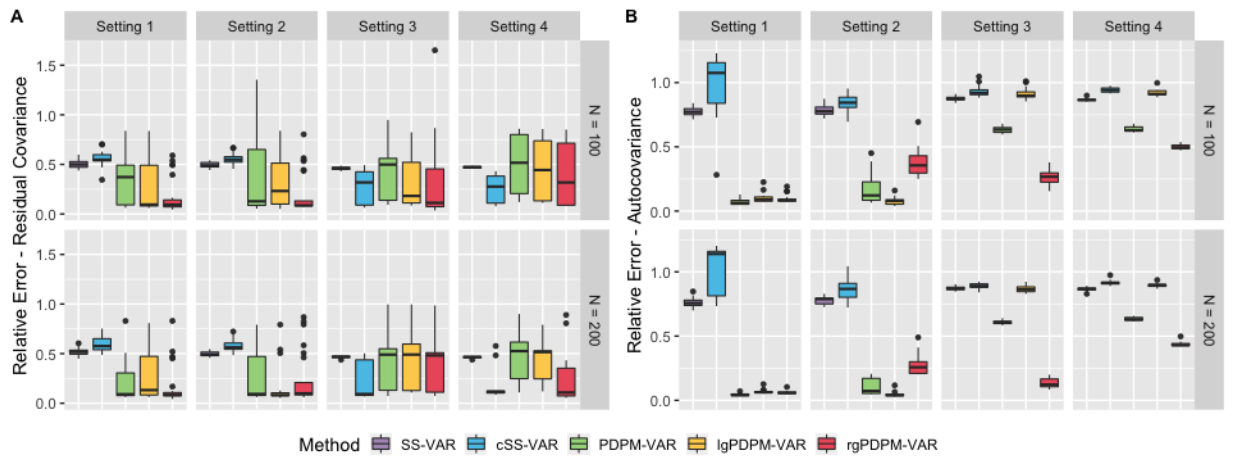


Figure 6: Simulation results for the $D = 40$, $T = 250$ case with sparsity level 0.75. Panel A and B display the relative L1 error for estimating the residual covariance and the subject-specific autocovariance matrices, respectively.

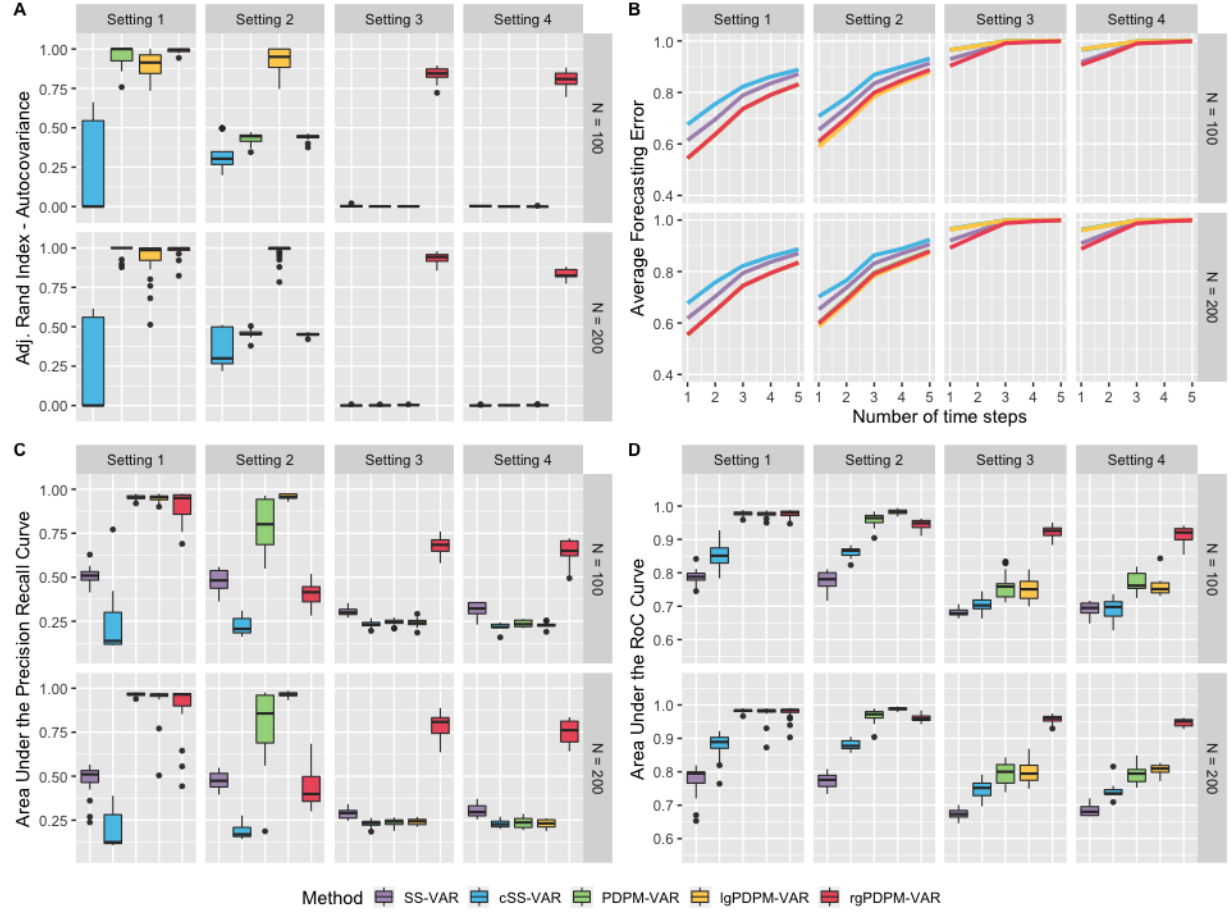


Figure 7: Simulation results for the $D = 40$, $T = 250$ case with sparsity level 0.9. Panel A displays the adjusted Rand index for clustering the autocovariance matrices. Panel B displays the forecasting error at 1–5 time steps. Panels C and D display the area under the PR and RoC curves for identifying non-zero elements of the autocovariance matrices.

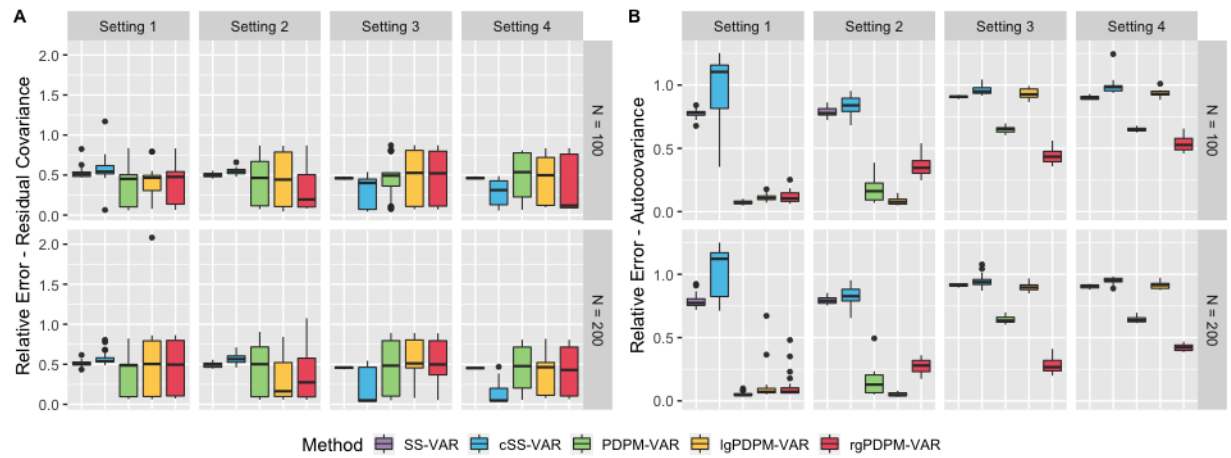


Figure 8: Simulation results for the $D = 40$, $T = 250$ case with sparsity level 0.9. Panel A and B display the relative L1 error for estimating the residual covariance and the subject-specific autocovariance matrices, respectively.

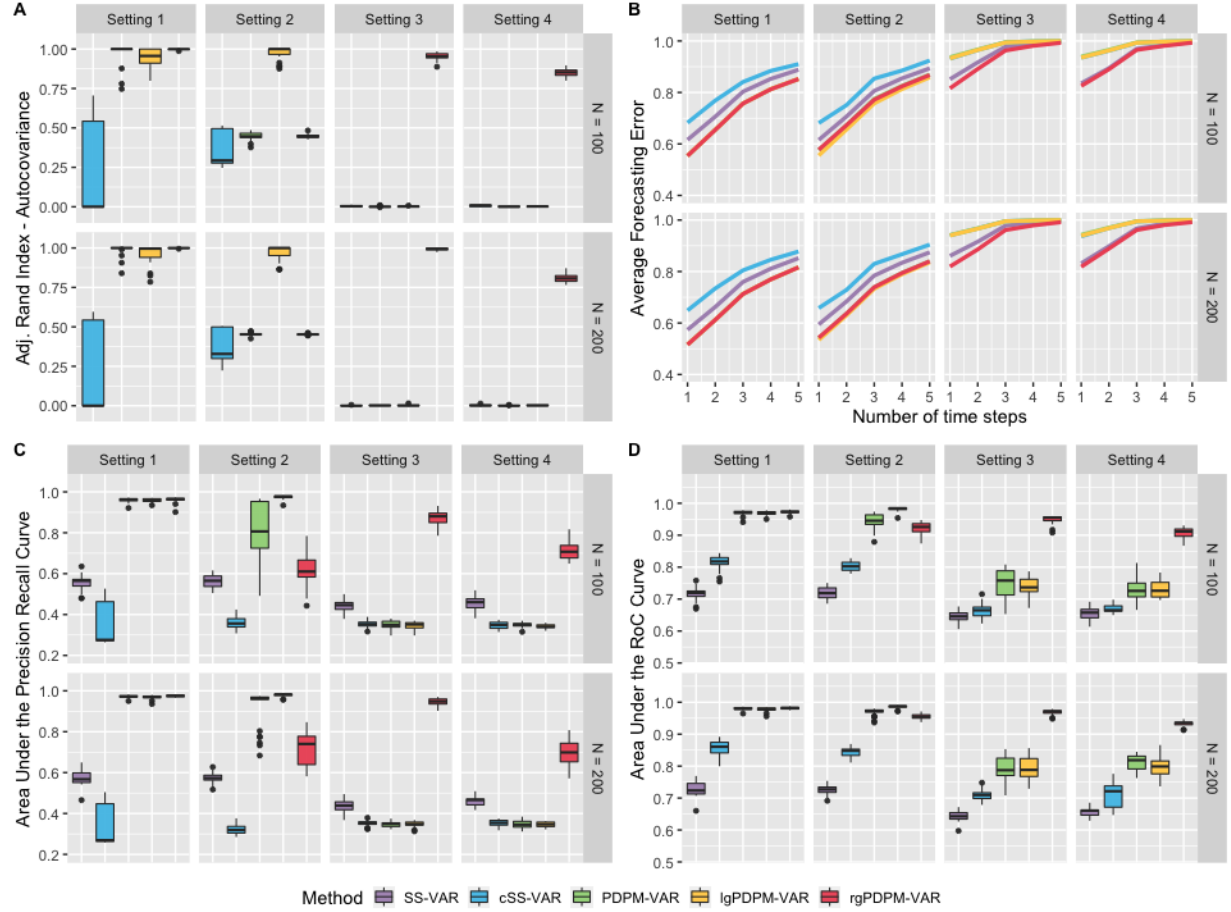


Figure 9: Simulation results for the $D = 40$, $T = 250, 350$ case with sparsity level 0.75. Panel A displays the adjusted Rand index for clustering the autocovariance matrices. Panel B displays the forecasting error at 1–5 time steps. Panels C and D display the area under the PR and RoC curves for identifying non-zero elements of the autocovariance matrices.

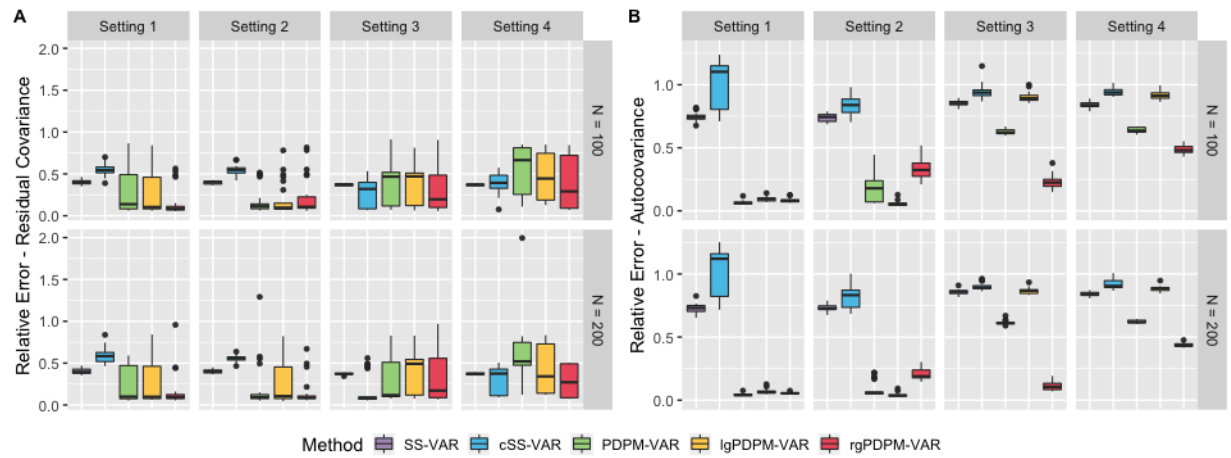


Figure 10: Simulation results for the $D = 40$, $T = 250, 350$ case with sparsity level 0.75. Panel A and B display the relative L1 error for estimating the residual covariance and the subject-specific autocovariance matrices, respectively.

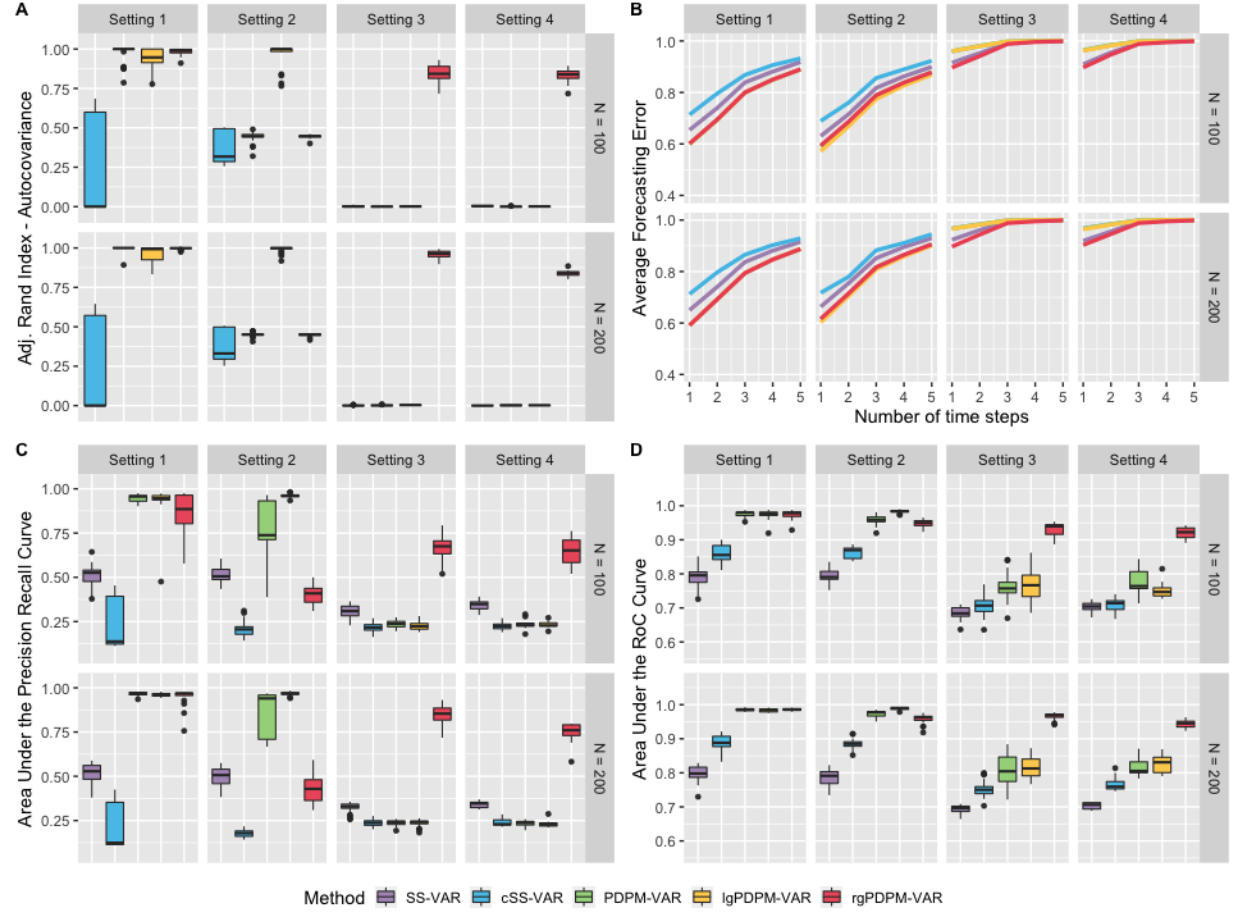


Figure 11: Simulation results for the $D = 40$, $T = 250, 350$ case with sparsity level 0.9. Panel A displays the adjusted Rand index for clustering the autocovariance matrices. Panel B displays the forecasting error at 1–5 time steps. Panels C and D display the area under the PR and RoC curves for identifying non-zero elements of the autocovariance matrices.

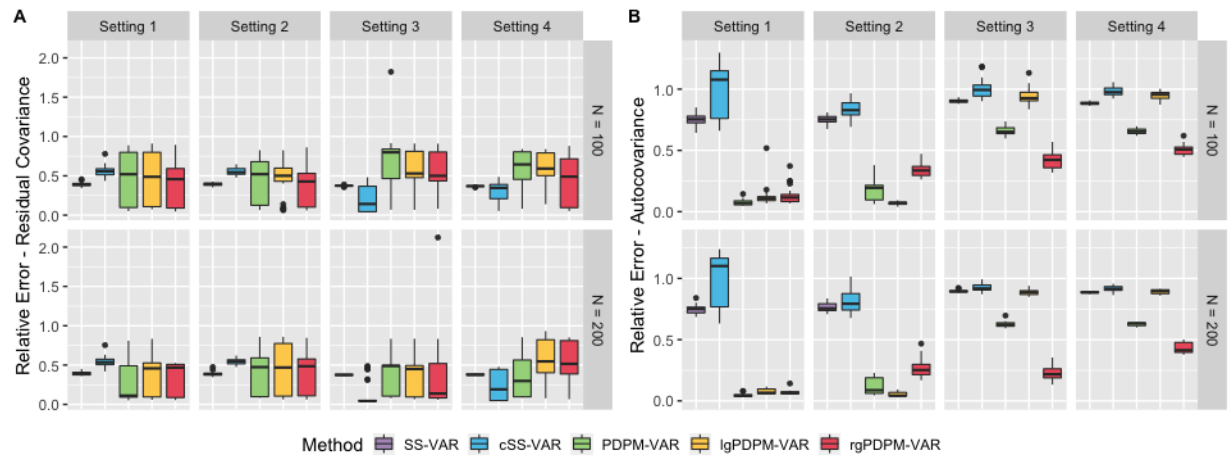


Figure 12: Simulation results for the $D = 40$, $T = 250, 350$ case with sparsity level 0.9. Panel A and B display the relative L1 error for estimating the residual covariance and the subject-specific autocovariance matrices, respectively.

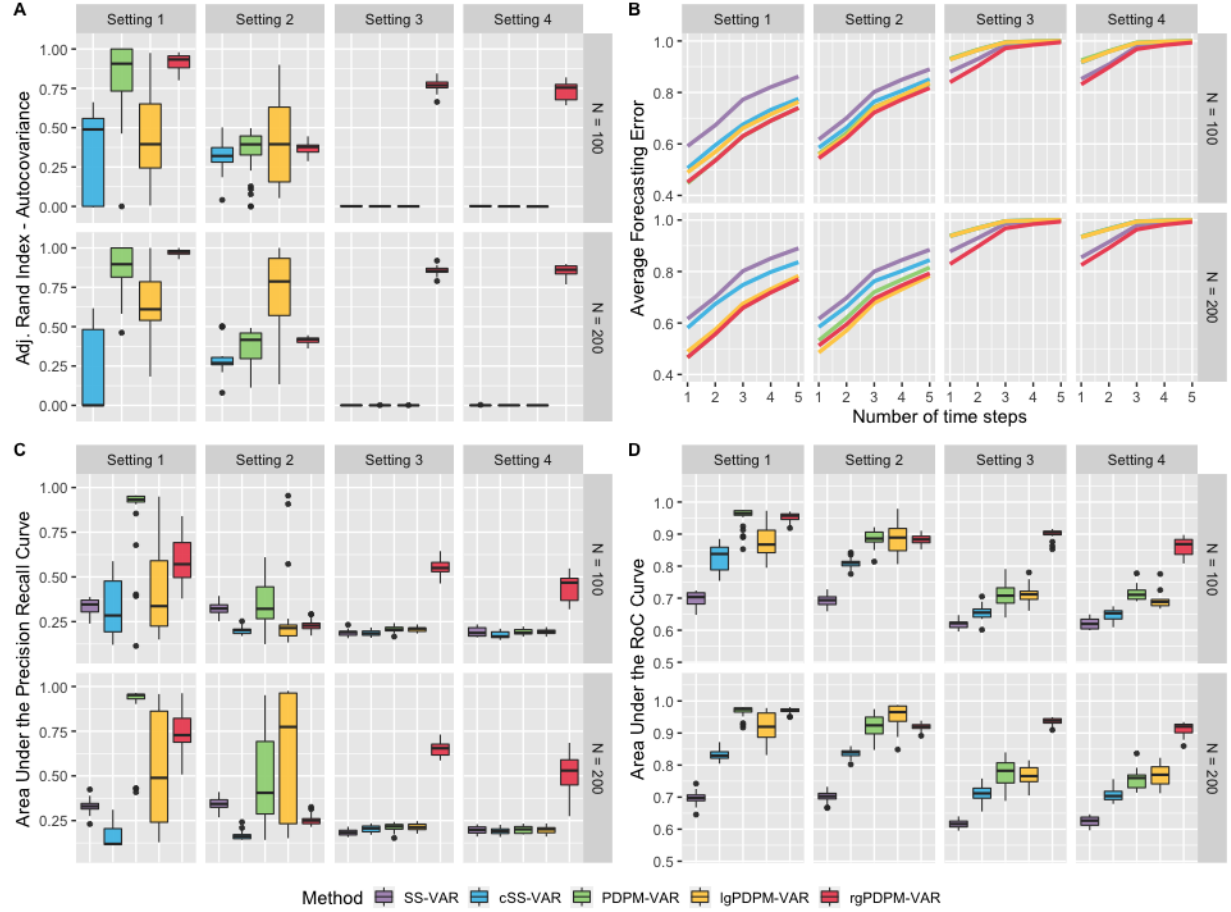


Figure 13: Simulation results for the $D = 100$, $T = 250$ case with sparsity level 0.9. Panel A displays the adjusted Rand index for clustering the autocovariance matrices. Panel B displays the forecasting error at 1–5 time steps. Panels C and D display the area under the PR and RoC curves for identifying non-zero elements of the autocovariance matrices.

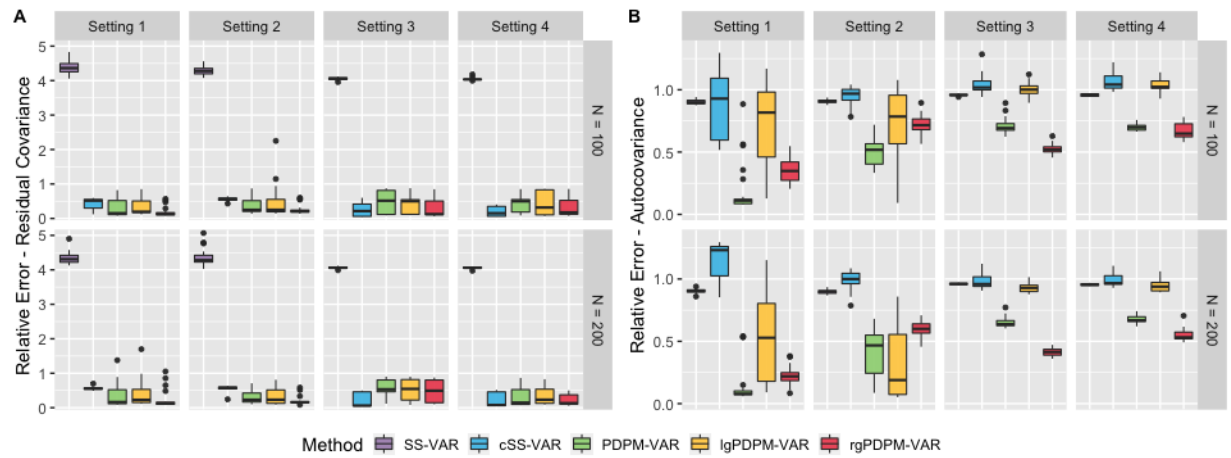


Figure 14: Simulation results for the $D = 100$, $T = 250$ case with sparsity level 0.9. Panel A and B display the relative L1 error for estimating the residual covariance and the subject-specific autocovariance matrices, respectively.

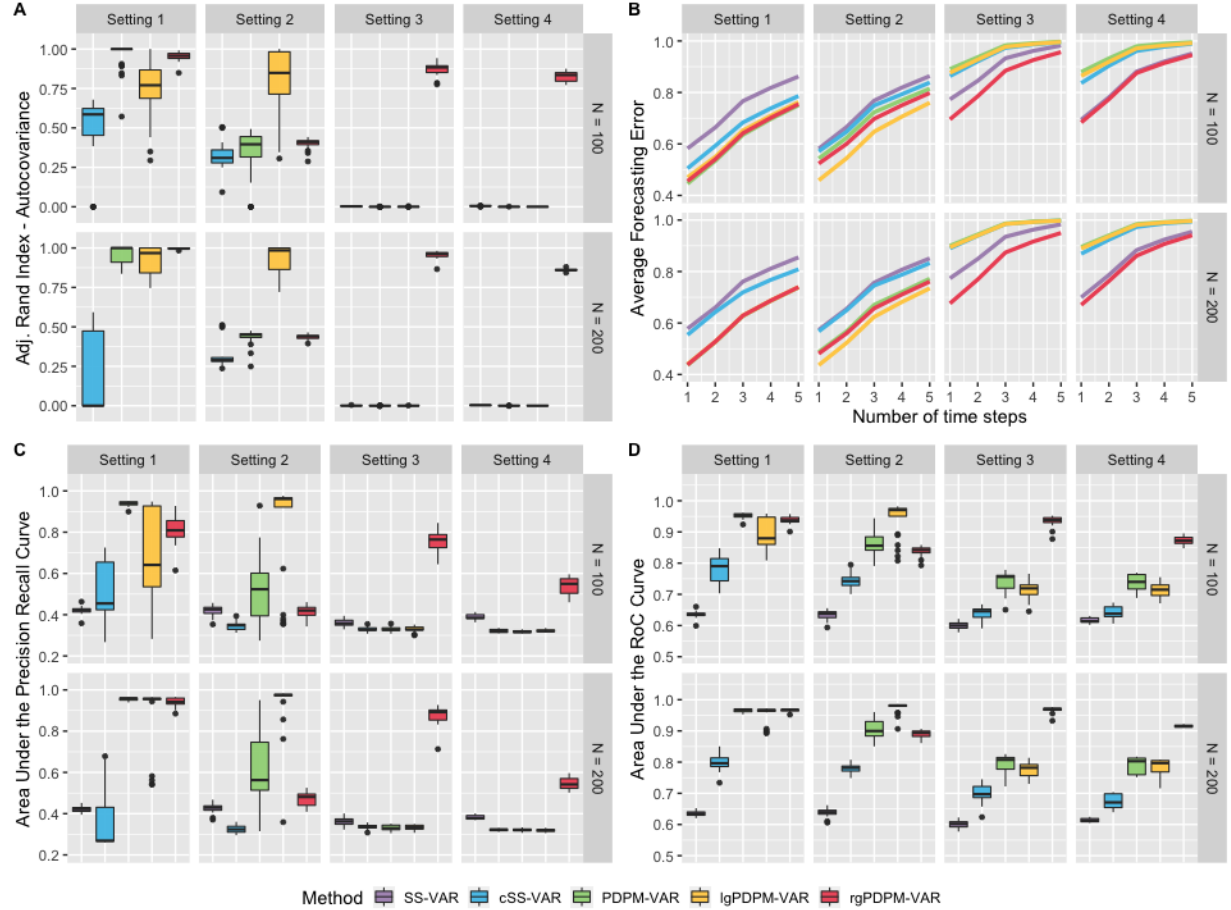


Figure 15: Simulation results for the $D = 100$, $T = 250, 350$ case with sparsity level 0.75. Panel A displays the adjusted Rand index for clustering the autocovariance matrices. Panel B displays the forecasting error at 1–5 time steps. Panels C and D display the area under the PR and RoC curves for identifying non-zero elements of the autocovariance matrices.

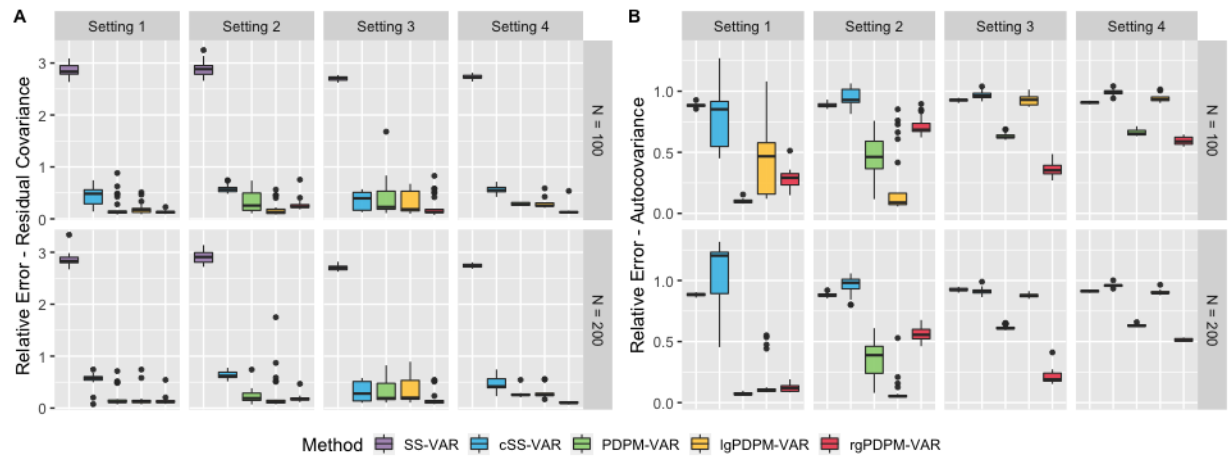


Figure 16: Simulation results for the $D = 100$, $T = 250, 350$ case with sparsity level 0.75. Panel A and B display the relative L1 error for estimating the residual covariance and the subject-specific autocovariance matrices, respectively.

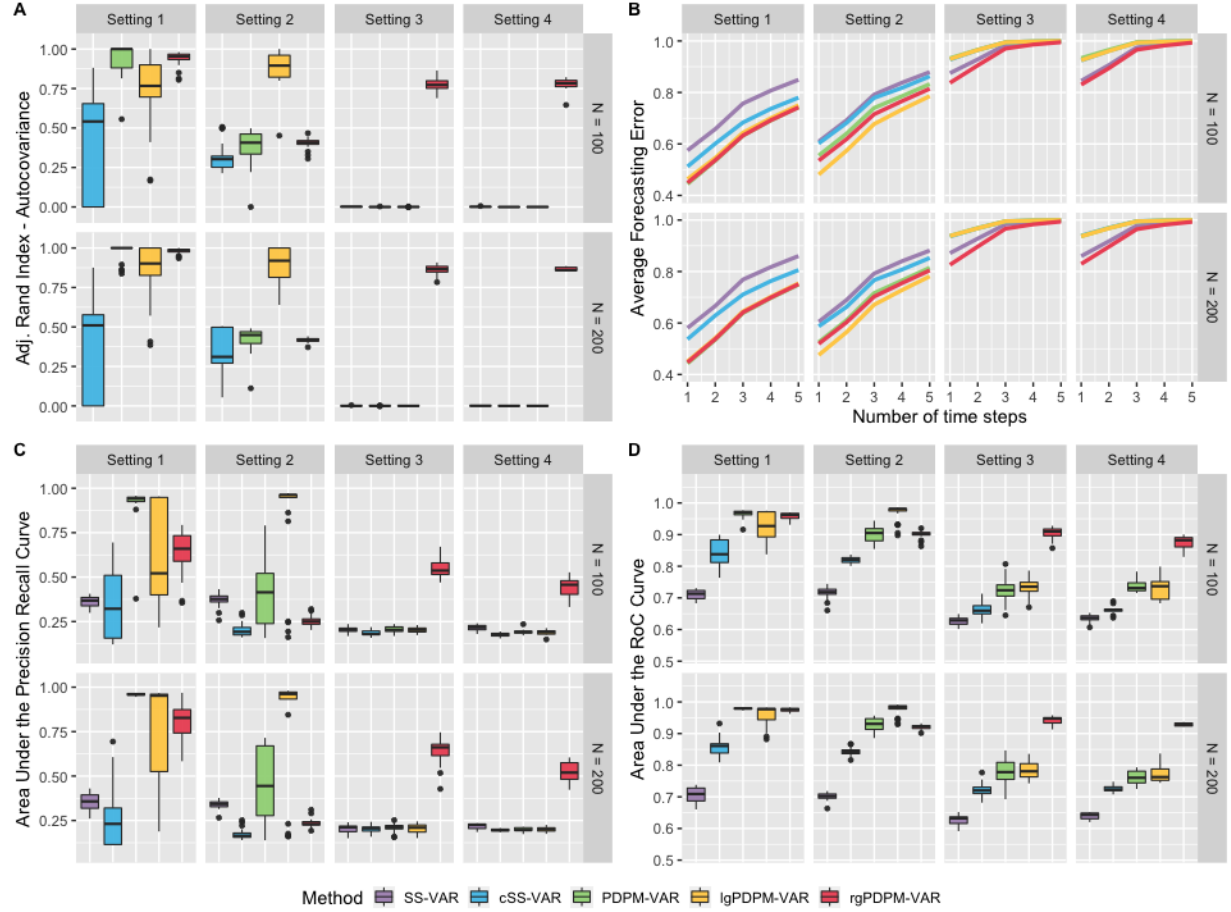


Figure 17: Simulation results for the $D = 100$, $T = 250, 350$ case with sparsity level 0.9. Panel A displays the adjusted Rand index for clustering the autocovariance matrices. Panel B displays the forecasting error at 1–5 time steps. Panels C and D display the area under the PR and RoC curves for identifying non-zero elements of the autocovariance matrices.

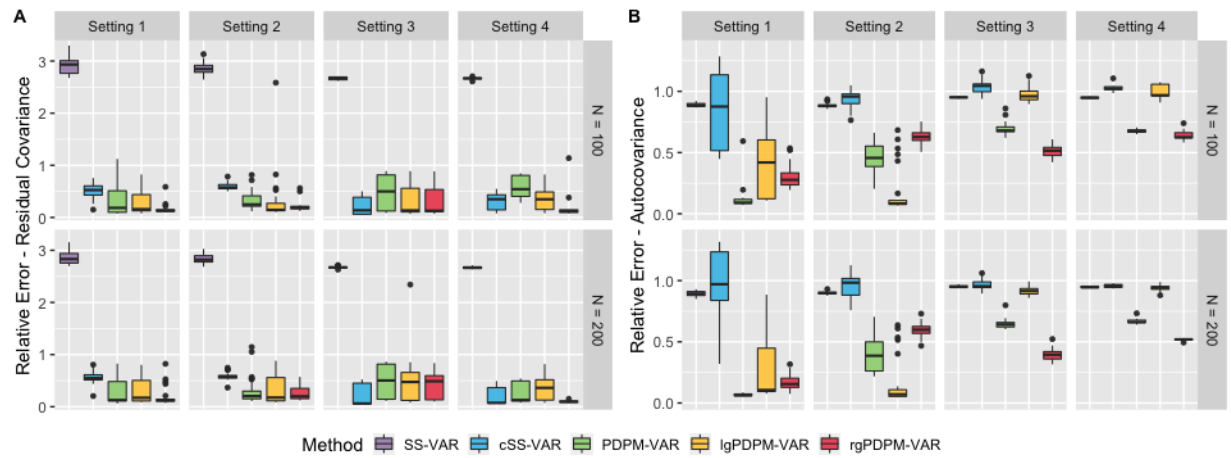


Figure 18: Simulation results for the $D = 100$, $T = 250, 350$ case with sparsity level 0.9. Panel A and B display the relative L1 error for estimating the residual covariance and the subject-specific autocovariance matrices, respectively.